BCS-based inversion methods within a multi-frequency framework

L. Poli, G. Oliveri, A. Massa

Abstract

In this report, the multi-frequency Multi-Task Bayesian Compressive Sensing (MT-BCS) technique is compared with the Single-Task Bayesian Compressive Sensing one (ST-BCS). The comparison shows how the first method, which concurrently handle the multi-frequency data taking into account the relationship between the correlated inverse problems associated to different illumination frequencies, provides better results. Moreover, single-frequency and multi-frequency approaches have been investigated.

Contents

Legenda

- SF-ST-BCS is the single-task Bayesian Compressive Sampling-based technique developed in [1] and working at a single frequency.
- MF-ST-BCS is the single-task Bayesian Compressive Sampling-based technique working at multiple frequencies.
- MF-MT-BCS is the multi-task Bayesian Compressive Sampling-based technique that exploits the correlation between multiple illumination frequencies.

1 Comparison with ST-BCS

1.1 Homogeneous Objects

1.1.1 Two Strips of Sides $l_1 = 0.16\lambda$, $l_2 = 0.50\lambda$

Goal: show the performances of the multi-frequency $MT - BCS$ when dealing with a sparse scatterer

- Number of frequencies F
- Number of Views: V
- Number of Measurements: M
- Number of Cells for the Inversion: N
- Number of Cells for the Direct solver: D
- Side of the investigation domain: L

Test Case Description

Direct solver:

- Square domain divided in $\sqrt{D} \times \sqrt{D}$ cells
- Domain side: $L = 3\lambda$ (at the central frequency)
- $D = 1296$ (discretization for the direct solver: $< \lambda/10$)

Investigation domain:

- Square domain divided in $\sqrt{N} \times \sqrt{N}$ cells
- $L = 3\lambda$
- $2ka = 2 \times \frac{2\pi}{\lambda} \times \frac{L\sqrt{2}}{2} = 6\pi\sqrt{2} = 26.65$
- $\#DOF = \frac{(2ka)^2}{2} = \frac{(2\times\frac{2\pi}{\lambda}\times\frac{L\sqrt{2}}{2})^2}{2} = 4\pi^2\left(\frac{L}{\lambda}\right)^2 = 4\pi^2 \times 9 \approx 355.3$
- N scelto in modo da essere vicino a $\#DOF$: $N = 324$ (18×18)

Measurement domain:

- Measurement points taken on a circle of radius $\rho = 3\lambda$ (at the central frequency)
- $M \approx 2ka \rightarrow M = 27$

Sources:

- $V = 1$ $(\theta = 0°)$
- Amplitude: $A = 1$ (plane waves)
- Number of Frequencies: $F = 11$
- Frequency Range: $I_F = [150\,Mhz\,:\,450MHz]$ - Frequency Step: $S_F = [30\,Mhz]$

Object:

- Two strips of sides $l_1 = 0.16\lambda$, $l_2 = 0.50\lambda$
- $\varepsilon_r = \in \{1.5,\, 2.0,\, 2.5,\, 3.0,\, 3.5,\, 4.0,\, 4.5,\, 5.0\}$
- $\sigma = 0$ [S/m]

MT-BCS parameters:

- Gamma prior on noise variance parameters: $\beta_1 = 6.5 \times 10^{-1}$, $\beta_2 = 5.8 \times 10^{-2}$
- Convergenze parameter: $\tau = 1.0 \times 10^{-8}$

Two Homogeneous Strips of Sides $l_1 = 0.16\lambda$, $l_2 = 0.50\lambda$ - $\varepsilon_r = 1.5$ - BCS Reconstructions Comparison

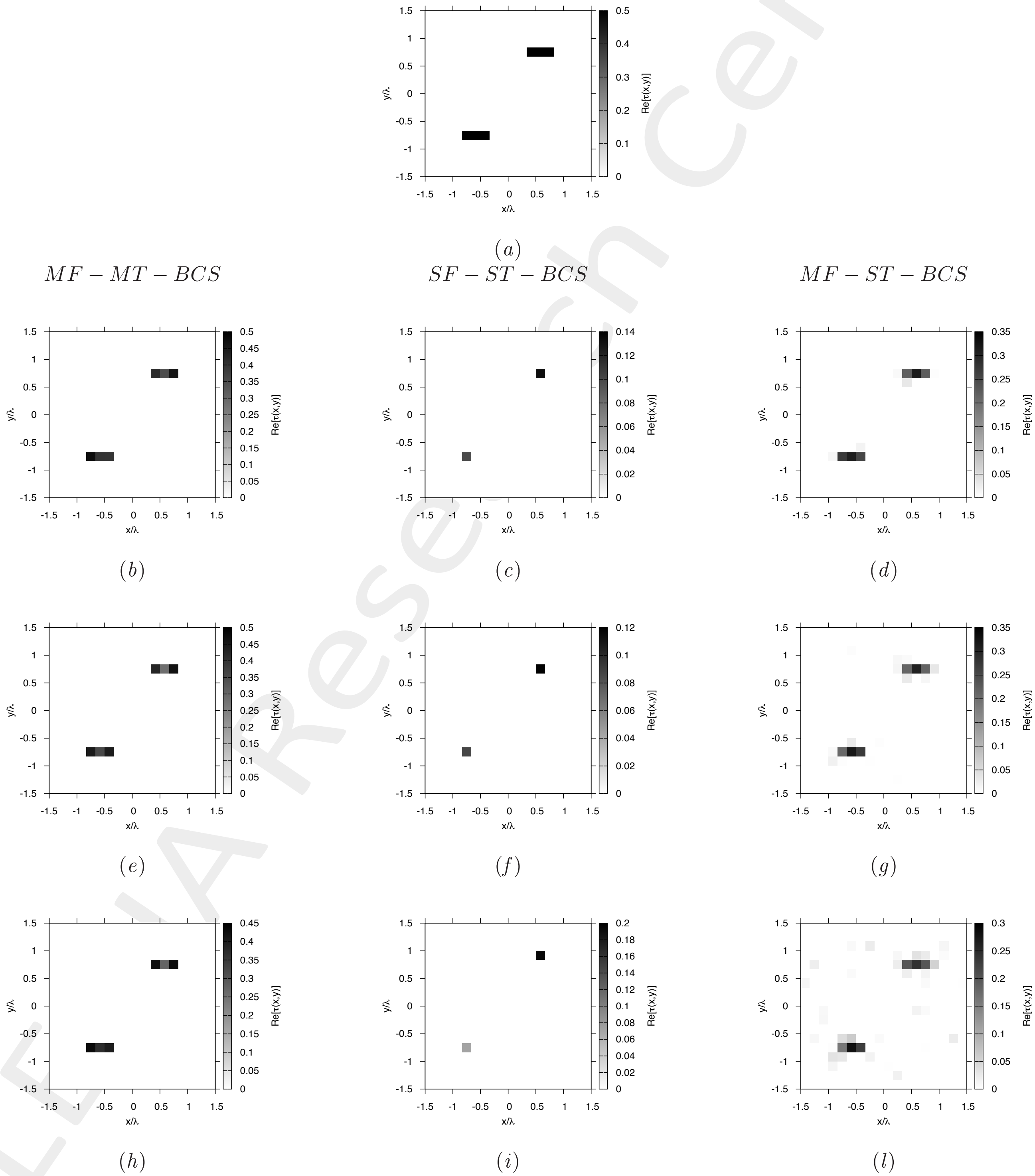

Figure 35. Actual object (a), $MF-MT-BCS$ reconstructed object $(b)(e)(h)$, $SF-ST-BCS$ $(c)(f)(i)$ and $MF-ST-BCS$ $(d)(g)(l)$ for $SNR = 50$ [dB] $(b)(c)(d)$, $SNR = 10$ [dB] $(e)(f)(g)$ and $SNR = 5$ [dB] $(h)(i)(l)$.

Two Homogeneous Strips of Sides $l_1 = 0.16\lambda$, $l_2 = 0.50\lambda$ - $\varepsilon_r = 2.0$ - BCS Reconstructions Comparison

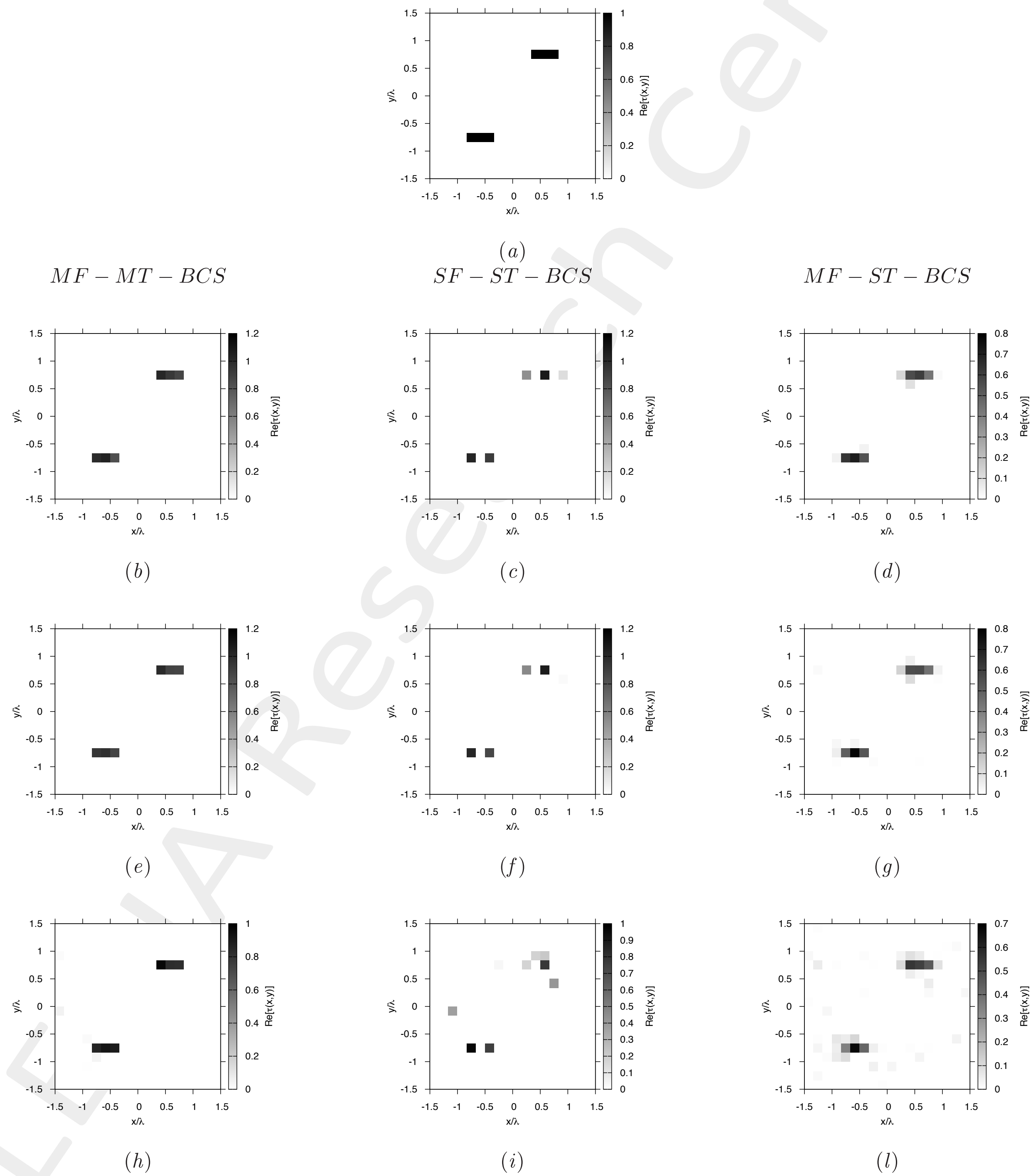

Figure 36. Actual object (a), $MF-MT-BCS$ reconstructed object $(b)(e)(h)$, $SF-ST-BCS$ $(c)(f)(i)$ and $MF-ST-BCS$ $(d)(g)(l)$ for $SNR = 50$ [dB] $(b)(c)(d)$, $SNR = 10$ [dB] $(e)(f)(g)$ and $SNR = 5$ [dB] $(h)(i)(l)$.

Two Homogeneous Strips of Sides $l_1 = 0.16\lambda$, $l_2 = 0.50\lambda$ - $\varepsilon_r = 3.0$ - BCS Reconstructions Comparison

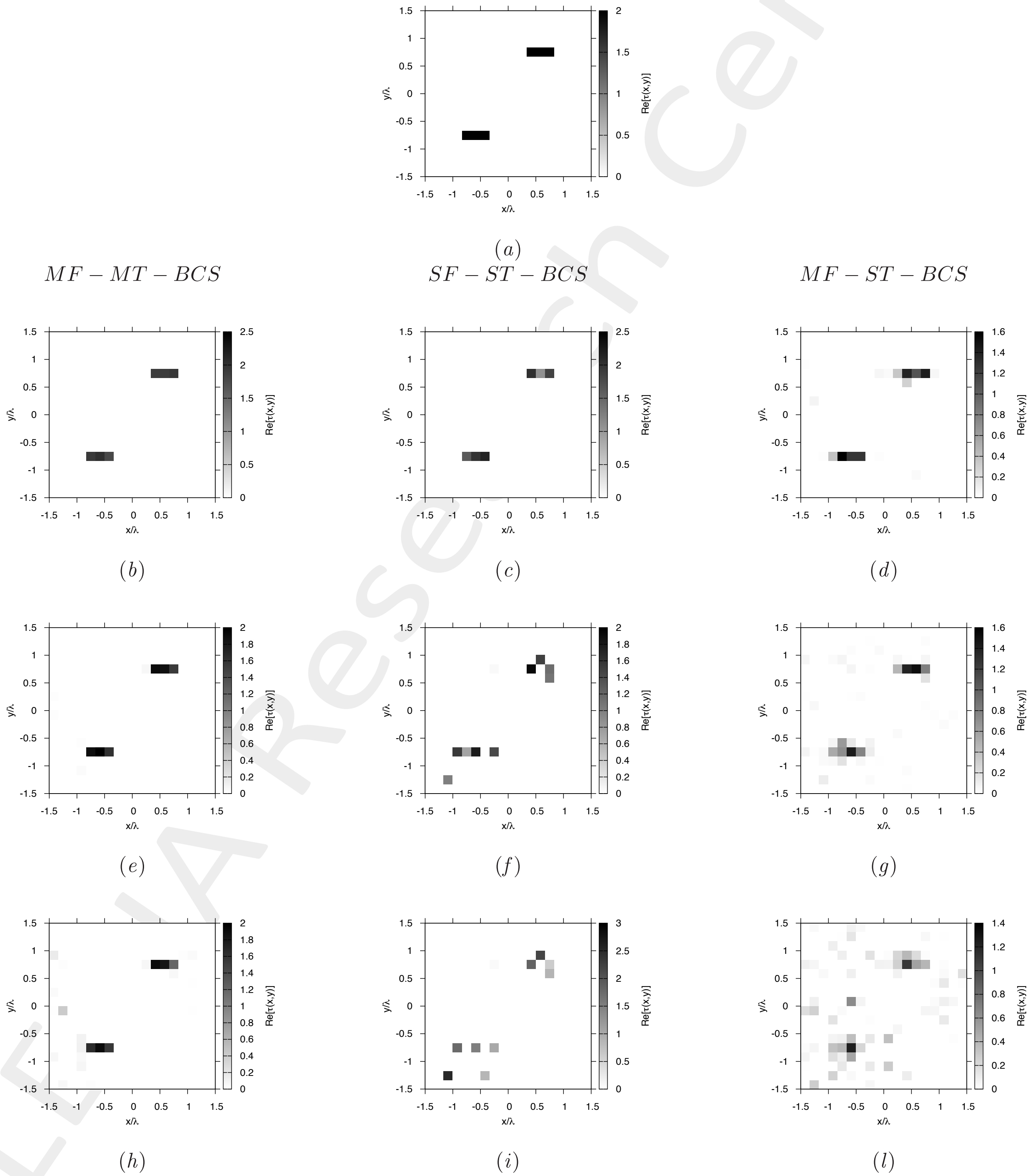

Figure 37. Actual object (a), $MF - MT - BCS$ reconstructed object $(b)(e)(h)$, $SF - ST - BCS$ $(c)(f)(i)$ and $MF - ST - BCS$ $(d)(g)(l)$ for $SNR = 50$ [dB] $(b)(c)(d)$, $SNR = 10$ [dB] $(e)(f)(g)$ and $SNR = 5$ [dB] $(h)(i)(l)$.

Two Homogeneous Strips of Sides $l_1 = 0.16\lambda$, $l_2 = 0.50\lambda$ - $\varepsilon_r = 4.0$ - BCS Reconstructions Comparison

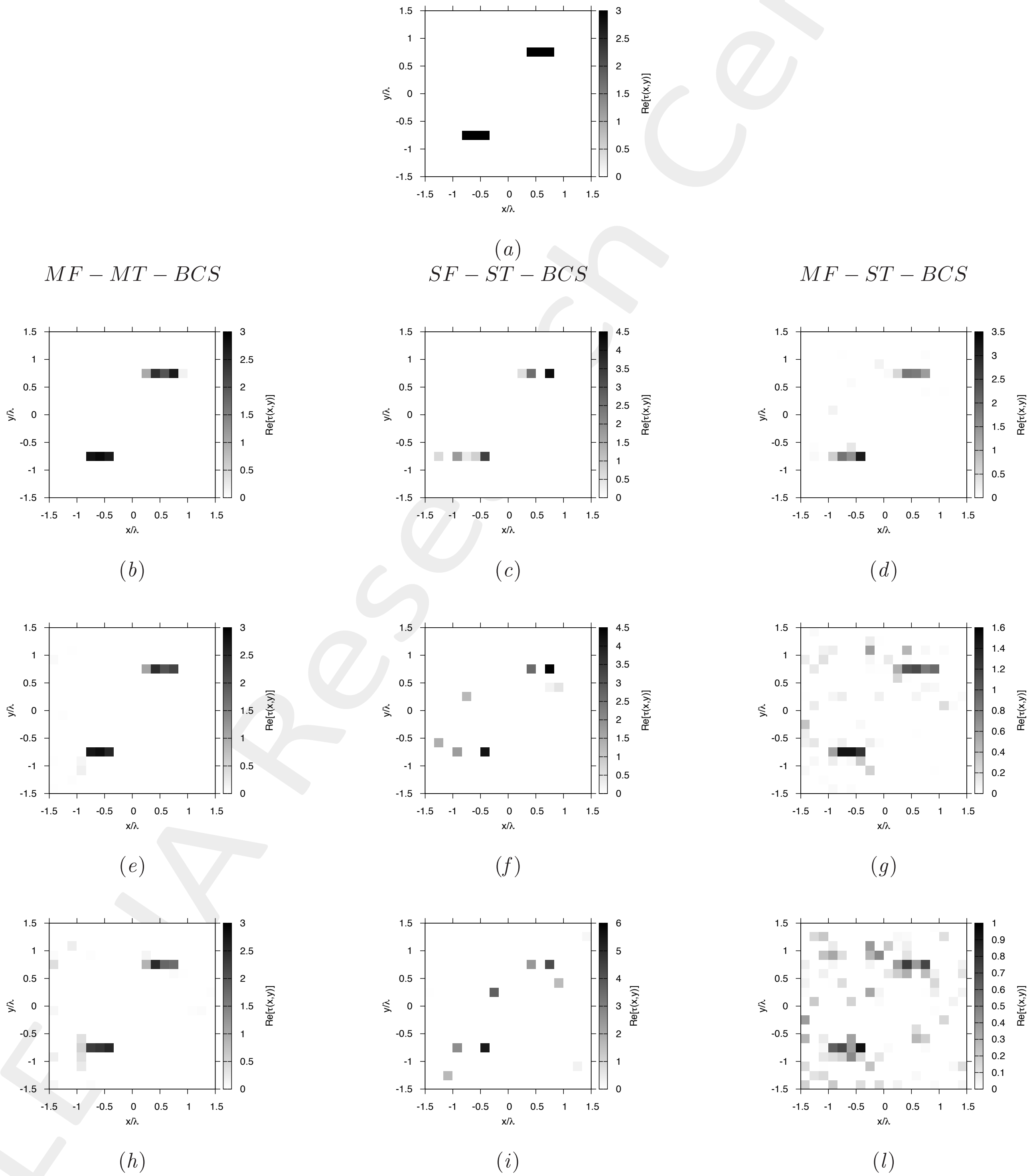

Figure 38. Actual object (a), $MF-MT-BCS$ reconstructed object $(b)(e)(h)$, $SF-ST-BCS$ $(c)(f)(i)$ and $MF-ST-BCS$ $(d)(g)(l)$ for $SNR = 50$ [dB] $(b)(c)(d)$, $SNR = 10$ [dB] $(e)(f)(g)$ and $SNR = 5$ [dB] $(h)(i)(l)$.

Two Homogeneous Strips of Sides $l_1 = 0.16\lambda$, $l_2 = 0.50\lambda$ - $\varepsilon_r = 5.0$ - BCS Reconstructions Comparison

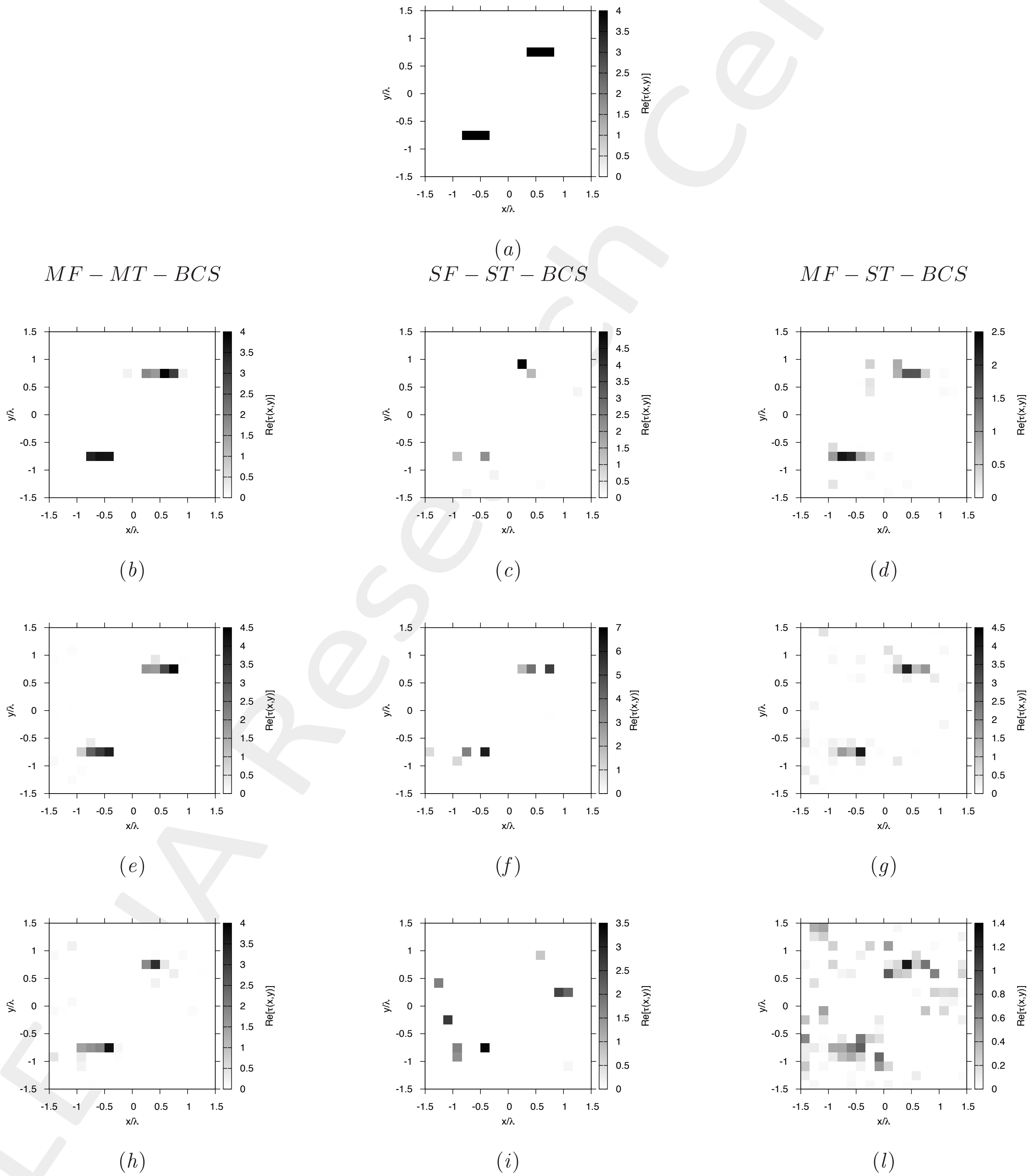

Figure 39. Actual object (a), $MF-MT-BCS$ reconstructed object $(b)(e)(h)$, $SF-ST-BCS$ $(c)(f)(i)$ and $MF-ST-BCS$ $(d)(g)(l)$ for $SNR = 50$ [dB] $(b)(c)(d)$, $SNR = 10$ [dB] $(e)(f)(g)$ and $SNR = 5$ [dB] $(h)(i)(l)$.

Two Homogeneous Strips of Sides $l_1 = 0.16\lambda$, $l_2 = 0.50\lambda$ - BCS Errors vs. ε_r Comparison

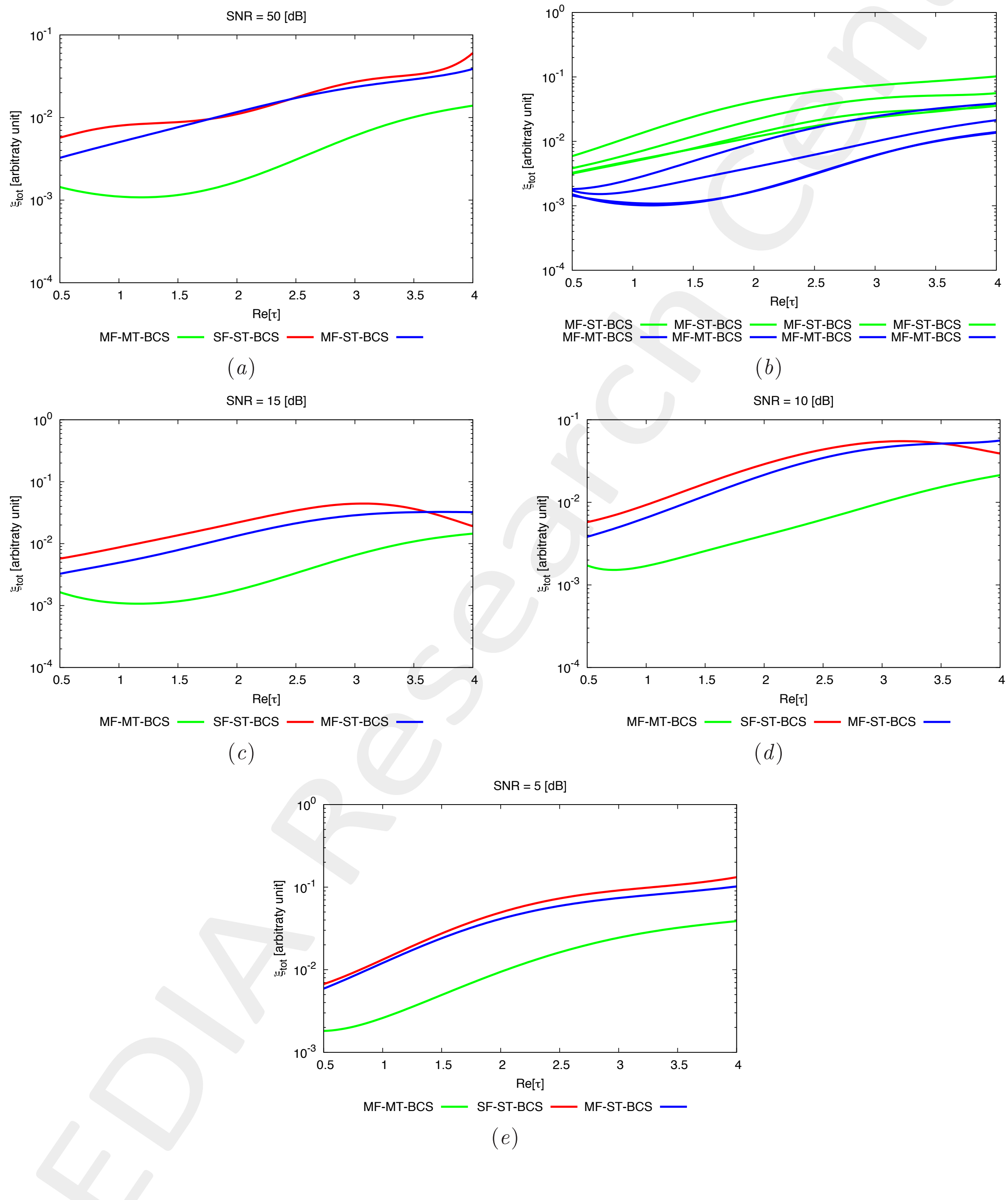

Figure 40. Behaviour of total error ξ_{tot} as a function of ε_r, for $SNR = 50$ [dB] (a), $SNR = 20$ [dB] (b), $SNR = 15$ [dB] (c), $SNR = 10$ [dB] (d) and $SNR = 5$ [dB] (e).

Two Homogeneous Strips of Sides $l_1 = 0.16\lambda$, $l_2 = 0.50\lambda$ - BCS Errors vs. SNR Comparison

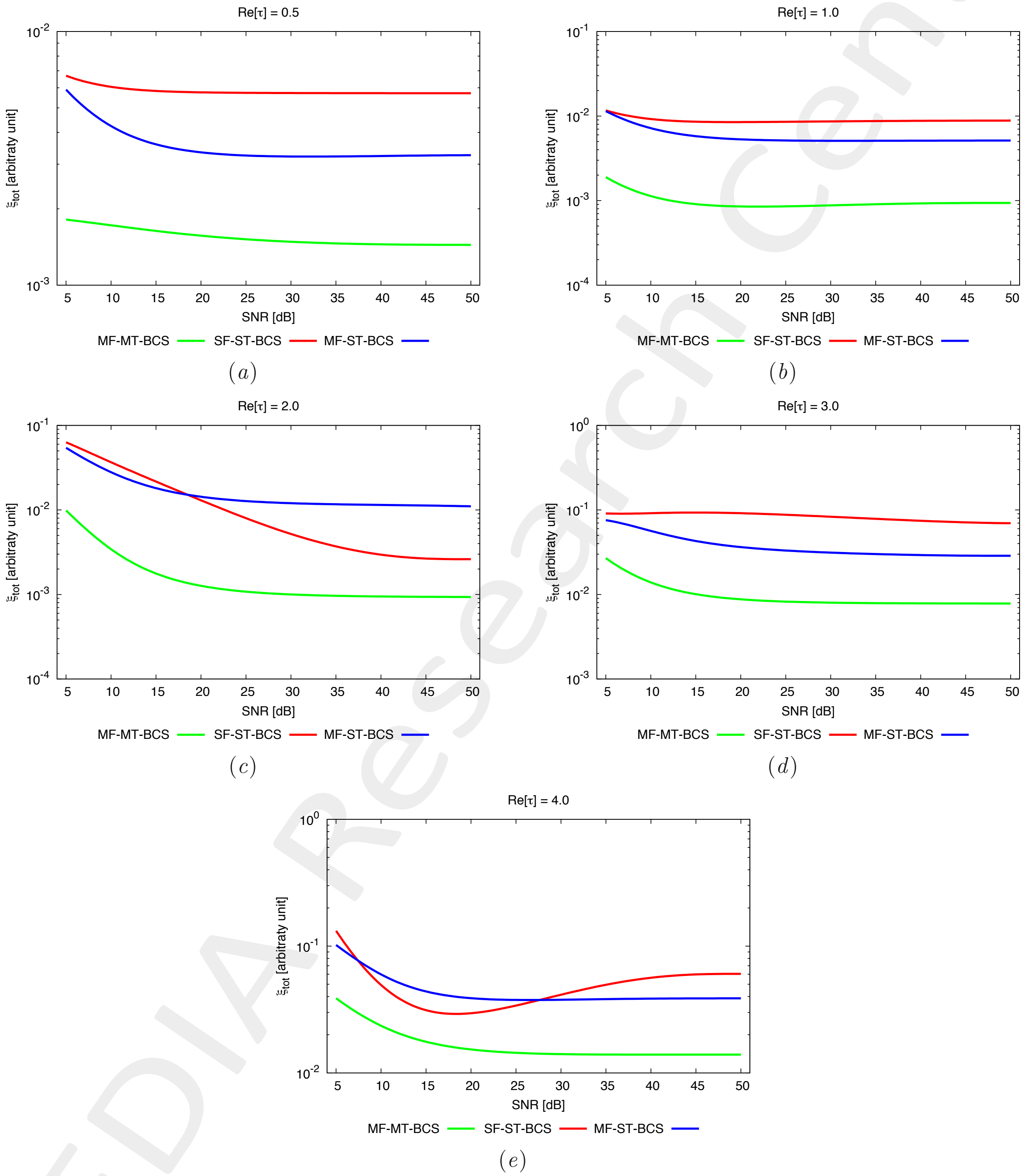

Figure 41. Behaviour of total error ξ_{tot} as a function of SNR, for $\varepsilon_r = 1.5$ [dB] (a), $\varepsilon_r = 2.0$ [dB] (b), $\varepsilon_r = 3.0$ [dB] (c), $\varepsilon_r = 4.0$ [dB] (d) and $\varepsilon_r = 5.0$ [dB] (e).

1.1.2 Eight Pixels of Side $l = 0.16\lambda$

Goal: show the performances of the multi-frequency $MT - BCS$ when dealing with a sparse scatterer

- Number of frequencies F
- Number of Views: V
- Number of Measurements: M
- Number of Cells for the Inversion: N
- Number of Cells for the Direct solver: D
- Side of the investigation domain: L

Test Case Description

Direct solver:

- Square domain divided in $\sqrt{D} \times \sqrt{D}$ cells
- Domain side: $L = 3\lambda$ (at the central frequency)
- $D = 1296$ (discretization for the direct solver: $< \lambda/10$)

Investigation domain:

- Square domain divided in $\sqrt{N} \times \sqrt{N}$ cells
- $L = 3\lambda$
- $2ka = 2 \times \frac{2\pi}{\lambda} \times \frac{L\sqrt{2}}{2} = 6\pi\sqrt{2} = 26.65$
- $\#DOF = \frac{(2ka)^2}{2} = \frac{(2\times\frac{2\pi}{\lambda}\times\frac{L\sqrt{2}}{2})^2}{2} = 4\pi^2\left(\frac{L}{\lambda}\right)^2 = 4\pi^2 \times 9 \approx 355.3$
- N scelto in modo da essere vicino a $\#DOF$: $N = 324$ (18×18)

Measurement domain:

- Measurement points taken on a circle of radius $\rho = 3\lambda$ (at the central frequency)
- $M \approx 2ka \rightarrow M = 27$

Sources:

- $V = 1$ $(\theta = 0°)$
- Amplitude: $A = 1$ (plane waves)
- Number of Frequencies: $F = 11$
- Frequency Range: $I_F = [150\,Mhz\,:\,450MHz]$ - Frequency Step: $S_F = [30\,Mhz]$

Object:

- Eight square cylinders of side $l = 0.16\lambda$
- $\varepsilon_r = \in \{1.5, 2.0, 2.5, 3.0, 3.5, 4.0, 4.5, 5.0\}$
- $\sigma = 0$ [S/m]

MT-BCS parameters:

- Gamma prior on noise variance parameters: $\beta_1 = 6.5 \times 10^{-1}$, $\beta_2 = 5.8 \times 10^{-2}$
- Convergenze parameter: $\tau = 1.0 \times 10^{-8}$

Eight Homogeneous Pixels of Side $l = 0.16\lambda$ - $\varepsilon_r = 1.5$ - BCS Reconstructions Comparison

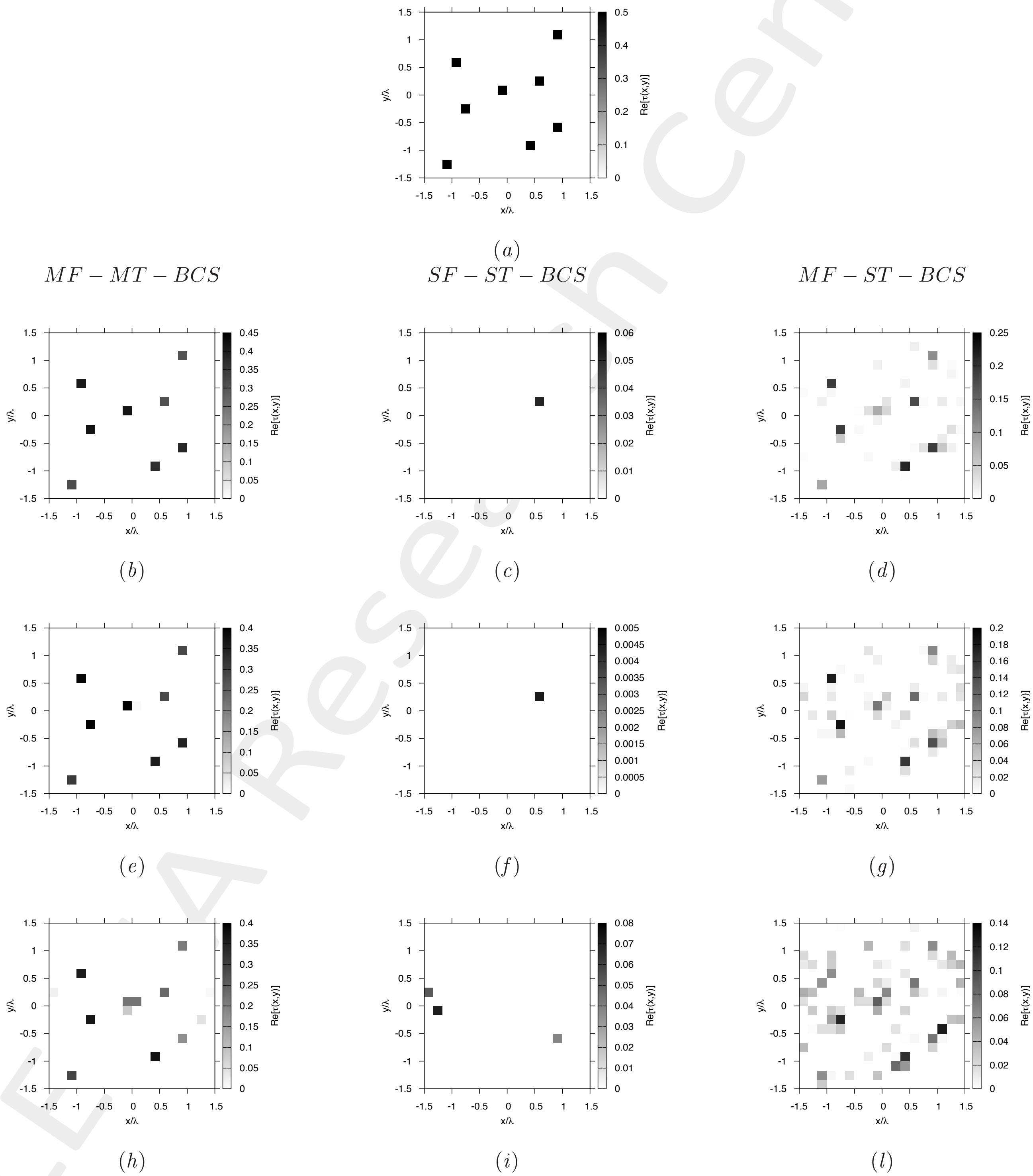

Figure 42. Actual object (a), $MF-MT-BCS$ reconstructed object $(b)(e)(h)$, $SF-ST-BCS$ $(c)(f)(i)$ and $MF-ST-BCS$ $(d)(g)(l)$ for $SNR = 50$ [dB] $(b)(c)(d)$, $SNR = 10$ [dB] $(e)(f)(g)$ and $SNR = 5$ [dB] $(h)(i)(l)$.

Eight Homogeneous Pixels of Side $l = 0.16\lambda$ - $\varepsilon_r = 2.0$ - BCS Reconstructions Comparison

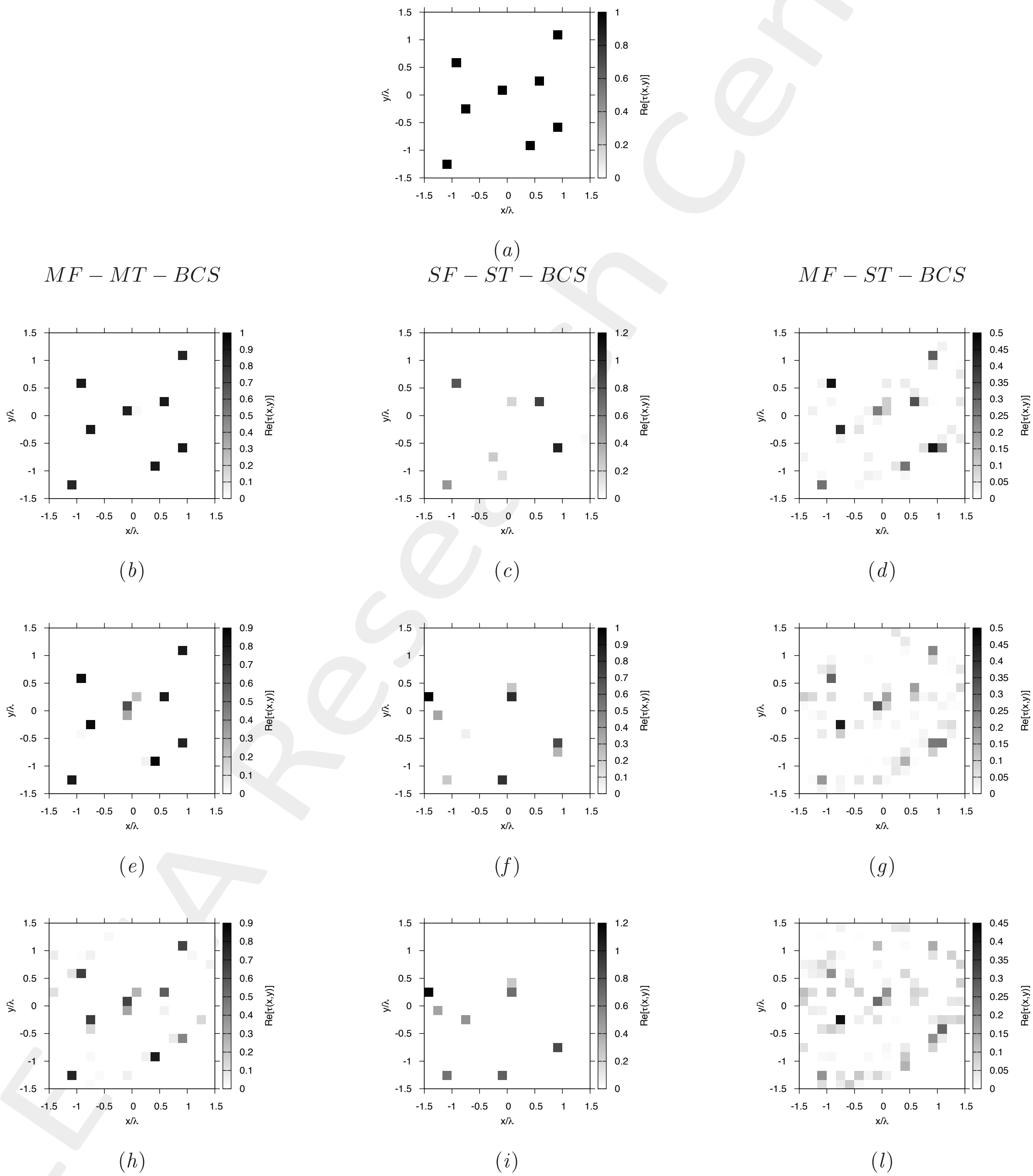

Figure 43. Actual object (a), $MF-MT-BCS$ reconstructed object $(b)(e)(h)$, $SF-ST-BCS$ $(c)(f)(i)$ and $MF-ST-BCS$ $(d)(g)(l)$ for $SNR = 50$ [dB] $(b)(c)(d)$, $SNR = 10$ [dB] $(e)(f)(g)$ and $SNR = 5$ [dB] $(h)(i)(l)$.

Eight Homogeneous Pixels of Side $l = 0.16\lambda$ - $\varepsilon_r = 3.0$ - BCS Reconstructions Comparison

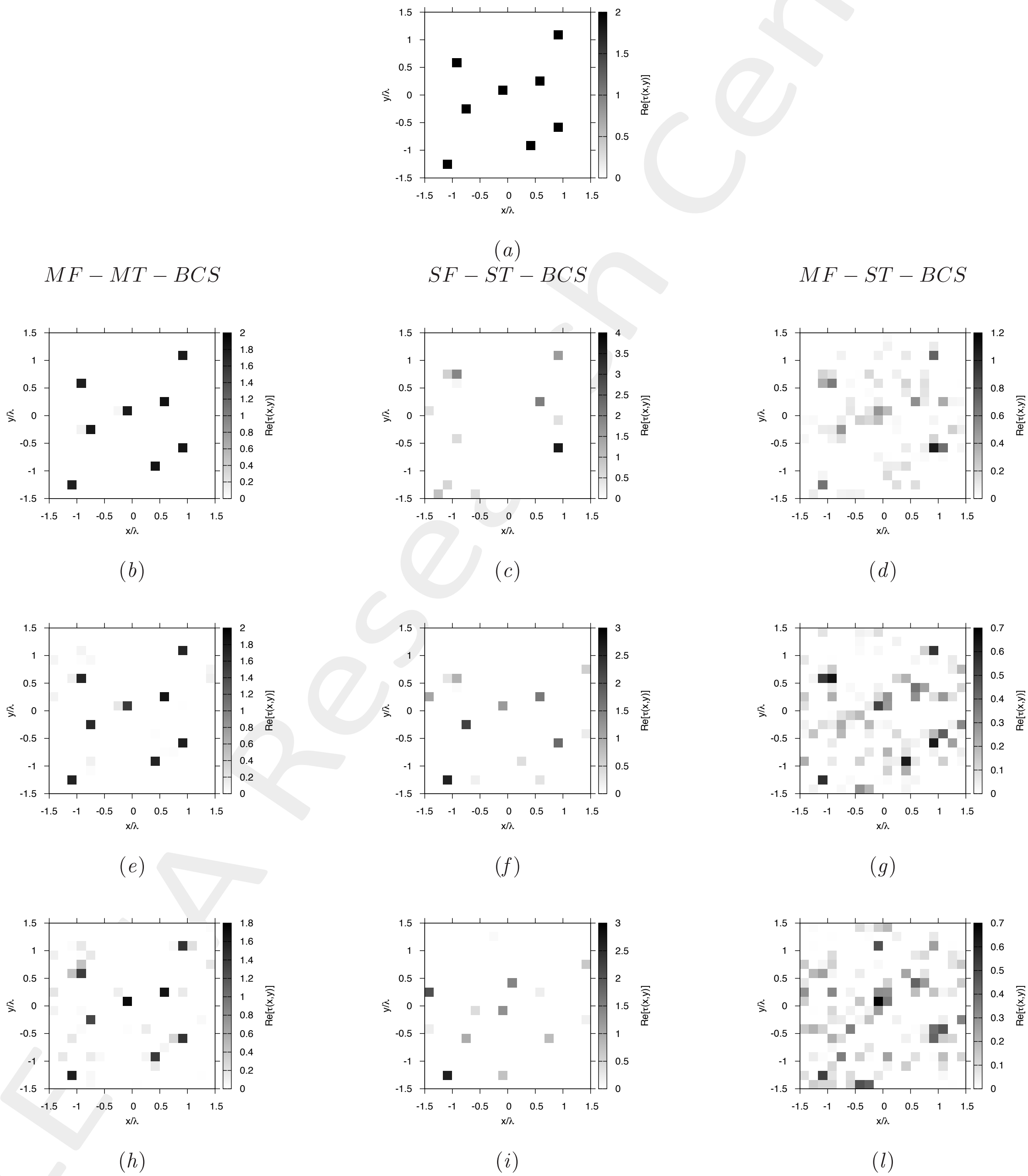

Figure 44. Actual object (a), $MF-MT-BCS$ reconstructed object $(b)(e)(h)$, $SF-ST-BCS$ $(c)(f)(i)$ and $MF-ST-BCS$ $(d)(g)(l)$ for $SNR = 50$ [dB] $(b)(c)(d)$, $SNR = 10$ [dB] $(e)(f)(g)$ and $SNR = 5$ [dB] $(h)(i)(l)$.

Eight Homogeneous Pixels of Side $l = 0.16\lambda$ - $\varepsilon_r = 4.0$ - BCS Reconstructions Comparison

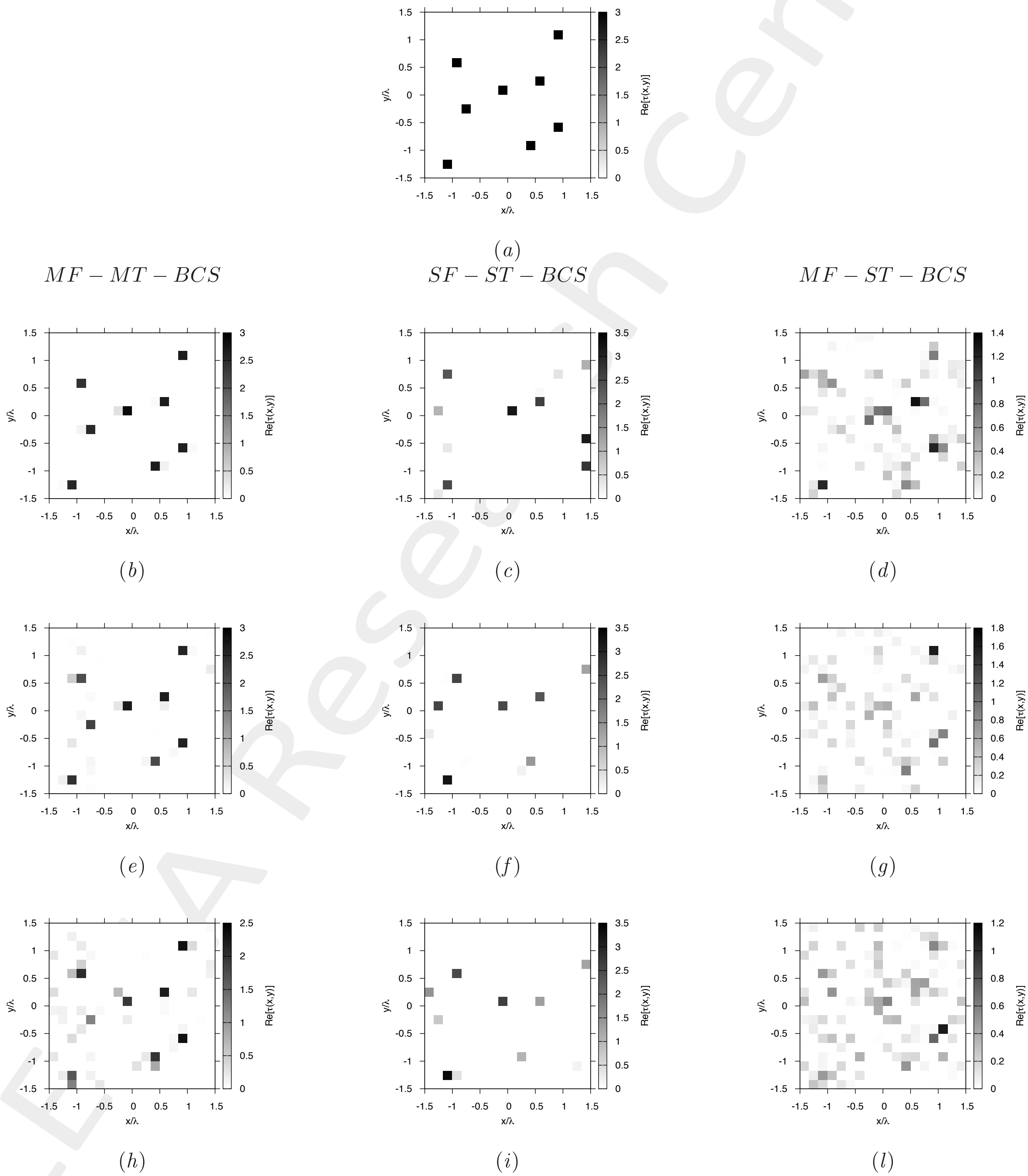

Figure 45. Actual object (a), $MF-MT-BCS$ reconstructed object $(b)(e)(h)$, $SF-ST-BCS$ $(c)(f)(i)$ and $MF-ST-BCS$ $(d)(g)(l)$ for $SNR = 50$ [dB] $(b)(c)(d)$, $SNR = 10$ [dB] $(e)(f)(g)$ and $SNR = 5$ [dB] $(h)(i)(l)$.

Eight Homogeneous Pixels of Side $l = 0.16\lambda$ - $\varepsilon_r = 5.0$ - BCS Reconstructions Comparison

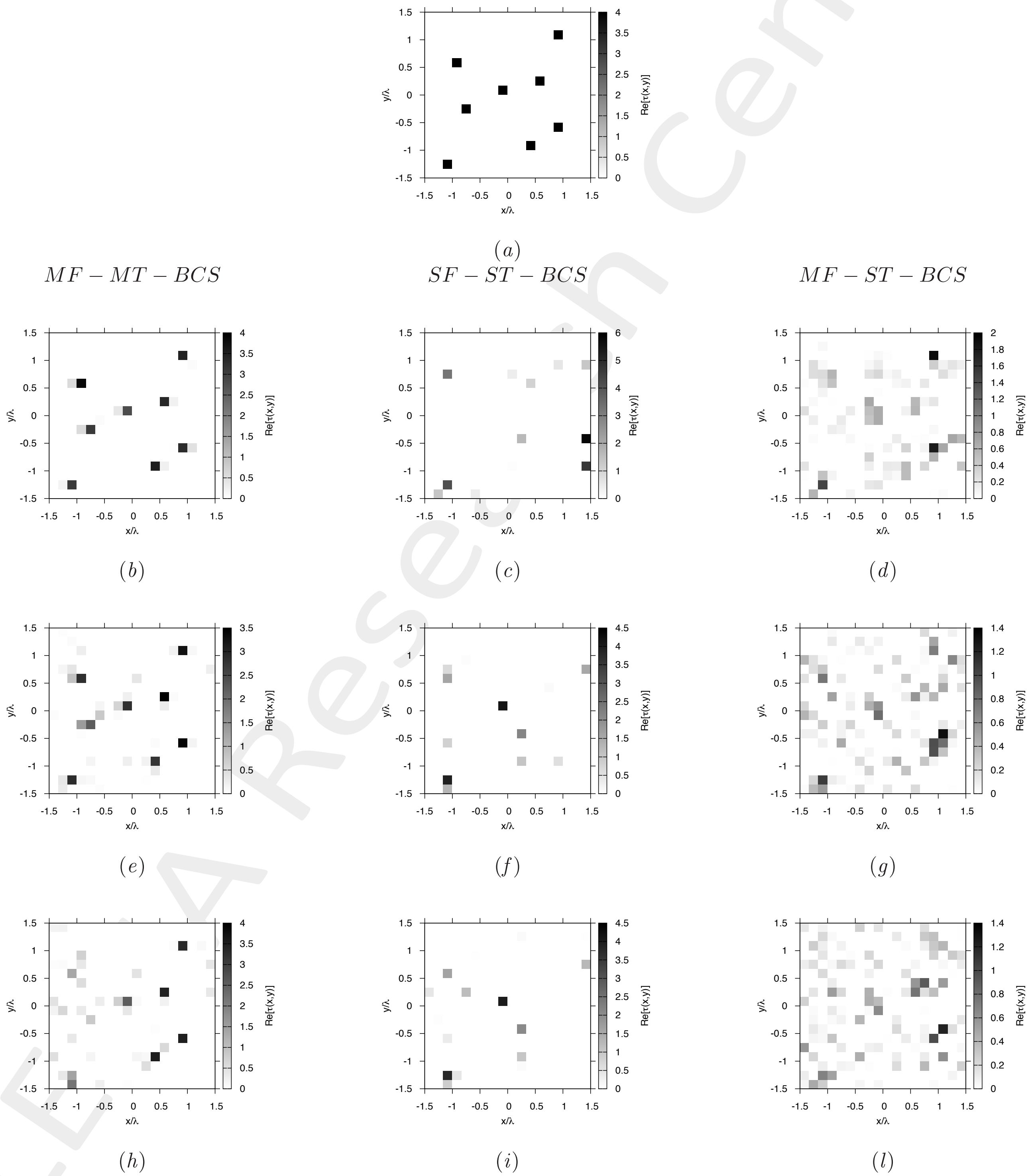

Figure 46. Actual object (a), $MF-MT-BCS$ reconstructed object $(b)(e)(h)$, $SF-ST-BCS$ $(c)(f)(i)$ and $MF-ST-BCS$ $(d)(g)(l)$ for $SNR = 50$ [dB] $(b)(c)(d)$, $SNR = 10$ [dB] $(e)(f)(g)$ and $SNR = 5$ [dB] $(h)(i)(l)$.

Eight Homogeneous Pixels of Side $l = 0.16\lambda$ - BCS Errors vs. ε_r Comparison

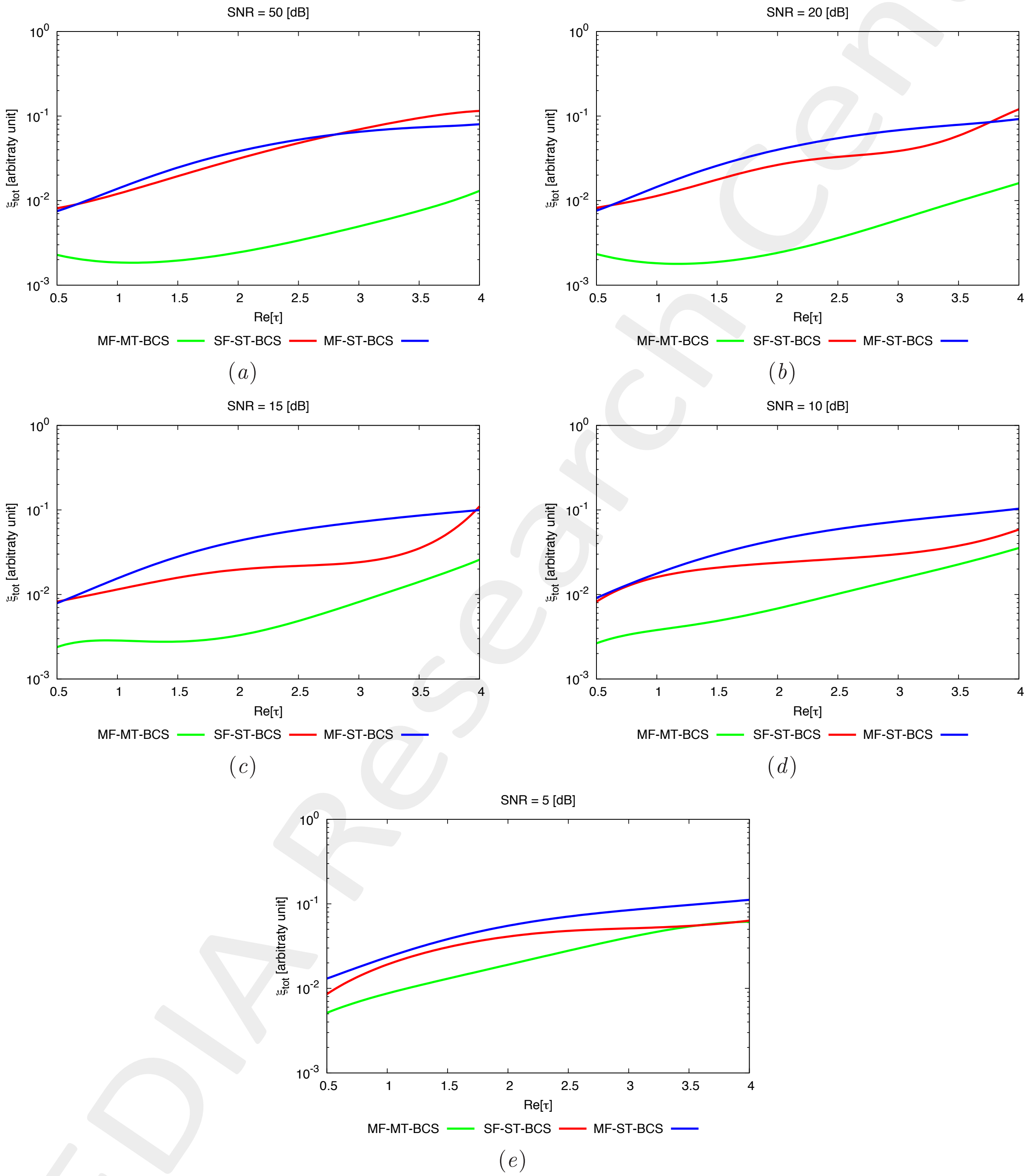

Figure 47. Behaviour of total error ξ_{tot} as a function of ε_r, for $SNR = 50$ [dB] (a), $SNR = 20$ [dB] (b), $SNR = 15$ [dB] (c), $SNR = 10$ [dB] (d) and $SNR = 5$ [dB] (e).

Eight Homogeneous Pixels of Side $l = 0.16\lambda$ - BCS Errors vs. SNR Comparison

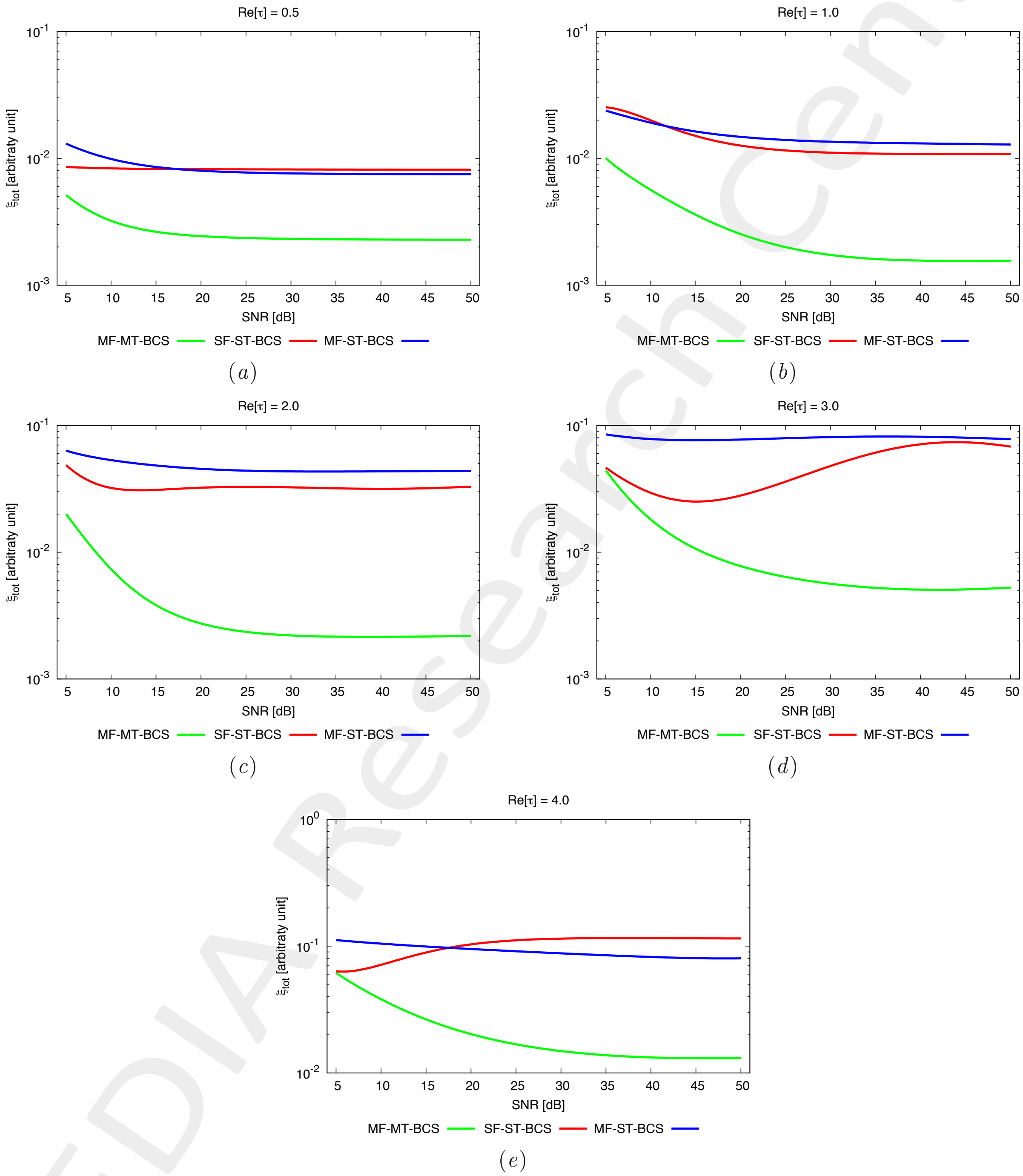

Figure 48. Behaviour of total error ξ_{tot} as a function of SNR, for $\varepsilon_r = 1.5$ [dB] (a), $\varepsilon_r = 2.0$ [dB] (b), $\varepsilon_r = 3.0$ [dB] (c), $\varepsilon_r = 4.0$ [dB] (d) and $\varepsilon_r = 5.0$ [dB] (e).

1.1.3 Rectangle of Sides $l_1 = 0.66\lambda$, $l_2 = 0.33\lambda$

Goal: show the performances of the multi-frequency $MT-BCS$ when dealing with a sparse scatterer

- Number of frequencies F
- Number of Views: V
- Number of Measurements: M
- Number of Cells for the Inversion: N
- Number of Cells for the Direct solver: D
- Side of the investigation domain: L

Test Case Description

Direct solver:

- Square domain divided in $\sqrt{D} \times \sqrt{D}$ cells
- Domain side: $L = 3\lambda$ (at the central frequency)
- $D = 1296$ (discretization for the direct solver: $< \lambda/10$)

Investigation domain:

- Square domain divided in $\sqrt{N} \times \sqrt{N}$ cells
- $L = 3\lambda$
- $2ka = 2 \times \frac{2\pi}{\lambda} \times \frac{L\sqrt{2}}{2} = 6\pi\sqrt{2} = 26.65$
- $\#DOF = \frac{(2ka)^2}{2} = \frac{(2\times\frac{2\pi}{\lambda}\times\frac{L\sqrt{2}}{2})^2}{2} = 4\pi^2\left(\frac{L}{\lambda}\right)^2 = 4\pi^2 \times 9 \approx 355.3$
- N scelto in modo da essere vicino a $\#DOF$: $N = 324$ (18×18)

Measurement domain:

- Measurement points taken on a circle of radius $\rho = 3\lambda$ (at the central frequency)
- $M \approx 2ka \rightarrow M = 27$

Sources:

- $V = 1$ $(\theta = 0°)$
- Amplitude: $A = 1$ (plane waves)
- Number of Frequencies: $F = 11$
- Frequency Range: $I_F = [150\,Mhz : 450MHz]$ - Frequency Step: $S_F = [30\,Mhz]$

Object:

- Rectangle of sides $l_1 = 0.33\lambda$, $l_2 = 0.66\lambda$
- $\varepsilon_r = \in \{1.5, 2.0, 2.5, 3.0, 3.5, 4.0, 4.5, 5.0\}$
- $\sigma = 0$ [S/m]

BCS parameters:

- Gamma prior on noise variance parameters: $\beta_1 = 6.5 \times 10^{-1}$, $\beta_2 = 5.8 \times 10^{-2}$
- Convergenze parameter: $\tau = 1.0 \times 10^{-8}$

Homogeneous Rectangle of Sides $l_1 = 0.66\lambda$, $l_2 = 0.33\lambda$ - $\varepsilon_r = 1.5$ - BCS Reconstructions Comparison

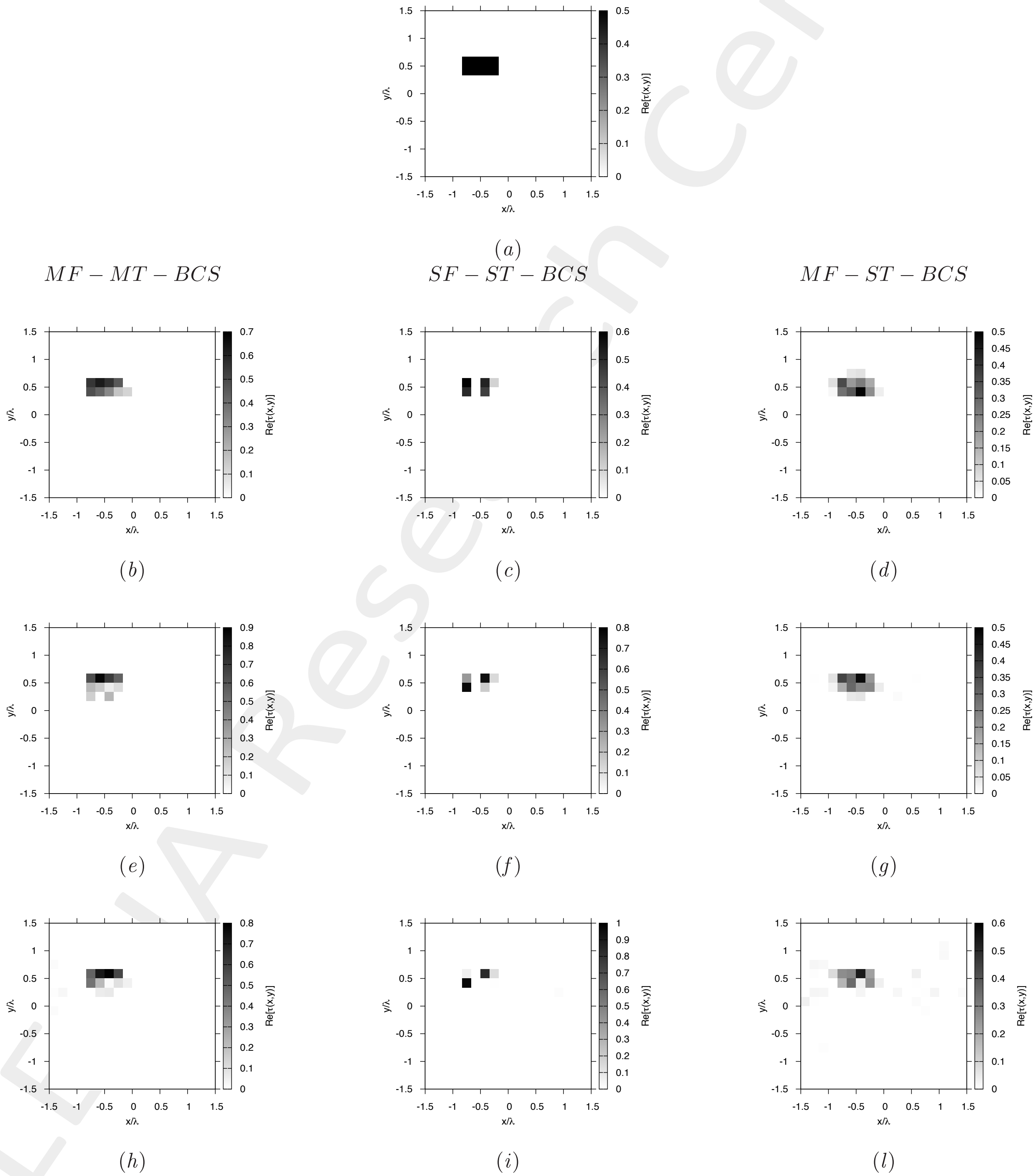

Figure 56. Actual object (a), $MF-MT-BCS$ reconstructed object $(b)(e)(h)$, $SF-ST-BCS$ $(c)(f)(i)$ and $MF-ST-BCS$ $(d)(g)(l)$ for $SNR = 50$ [dB] $(b)(c)(d)$, $SNR = 10$ [dB] $(e)(f)(g)$ and $SNR = 5$ [dB] $(h)(i)(l)$.

Homogeneous Rectangle of Sides $l_1 = 0.66\lambda$, $l_2 = 0.33\lambda$ - $\varepsilon_r = 2.0$ - BCS Reconstructions Comparison

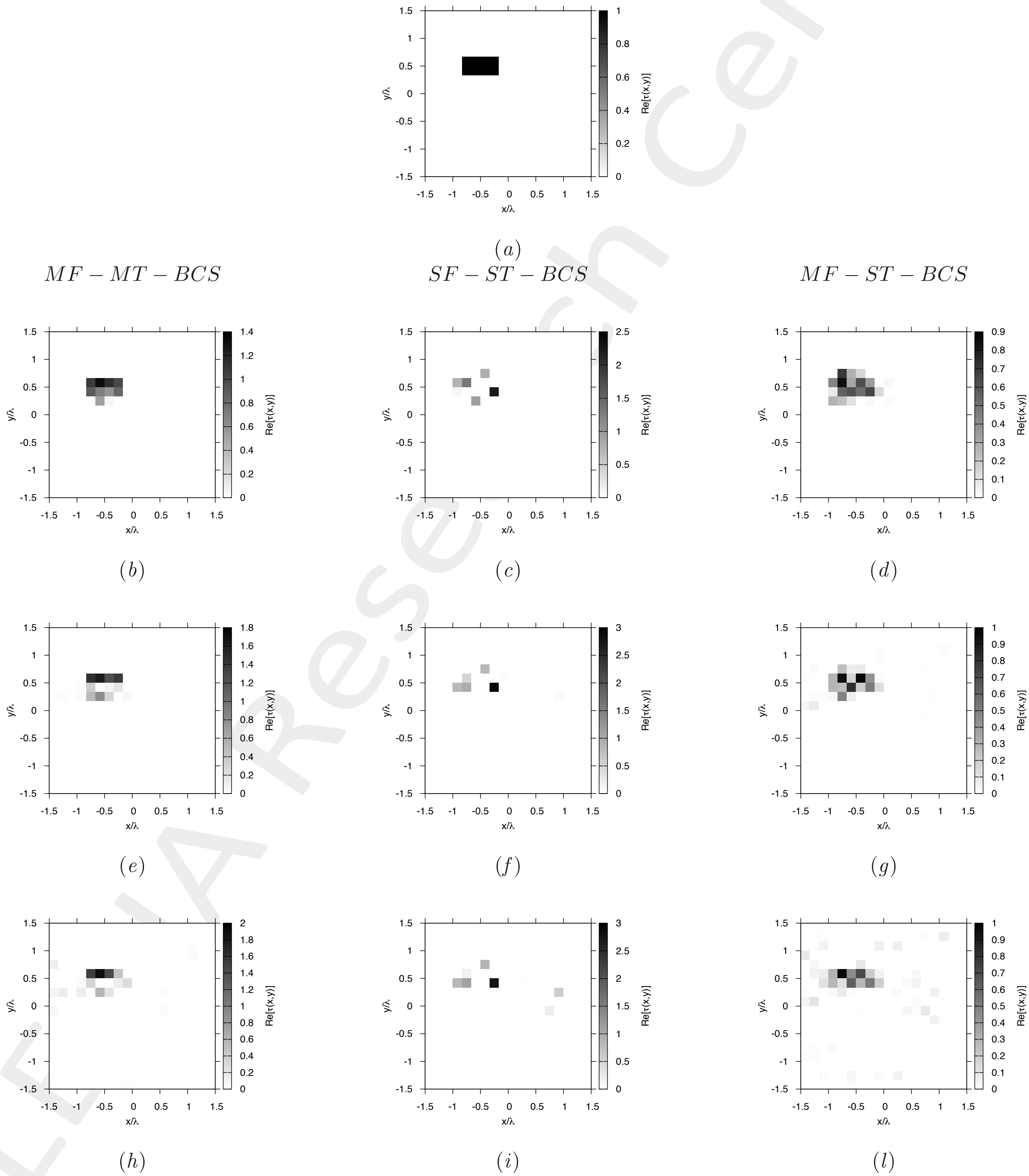

Figure 57. Actual object (a), $MF-MT-BCS$ reconstructed object $(b)(e)(h)$, $SF-ST-BCS$ $(c)(f)(i)$ and $MF-ST-BCS$ $(d)(g)(l)$ for $SNR=50$ [dB] $(b)(c)(d)$, $SNR=10$ [dB] $(e)(f)(g)$ and $SNR=5$ [dB] $(h)(i)(l)$.

Homogeneous Rectangle of Sides $l_1 = 0.66\lambda$, $l_2 = 0.33\lambda$ - $\varepsilon_r = 3.0$ - BCS Reconstructions Comparison

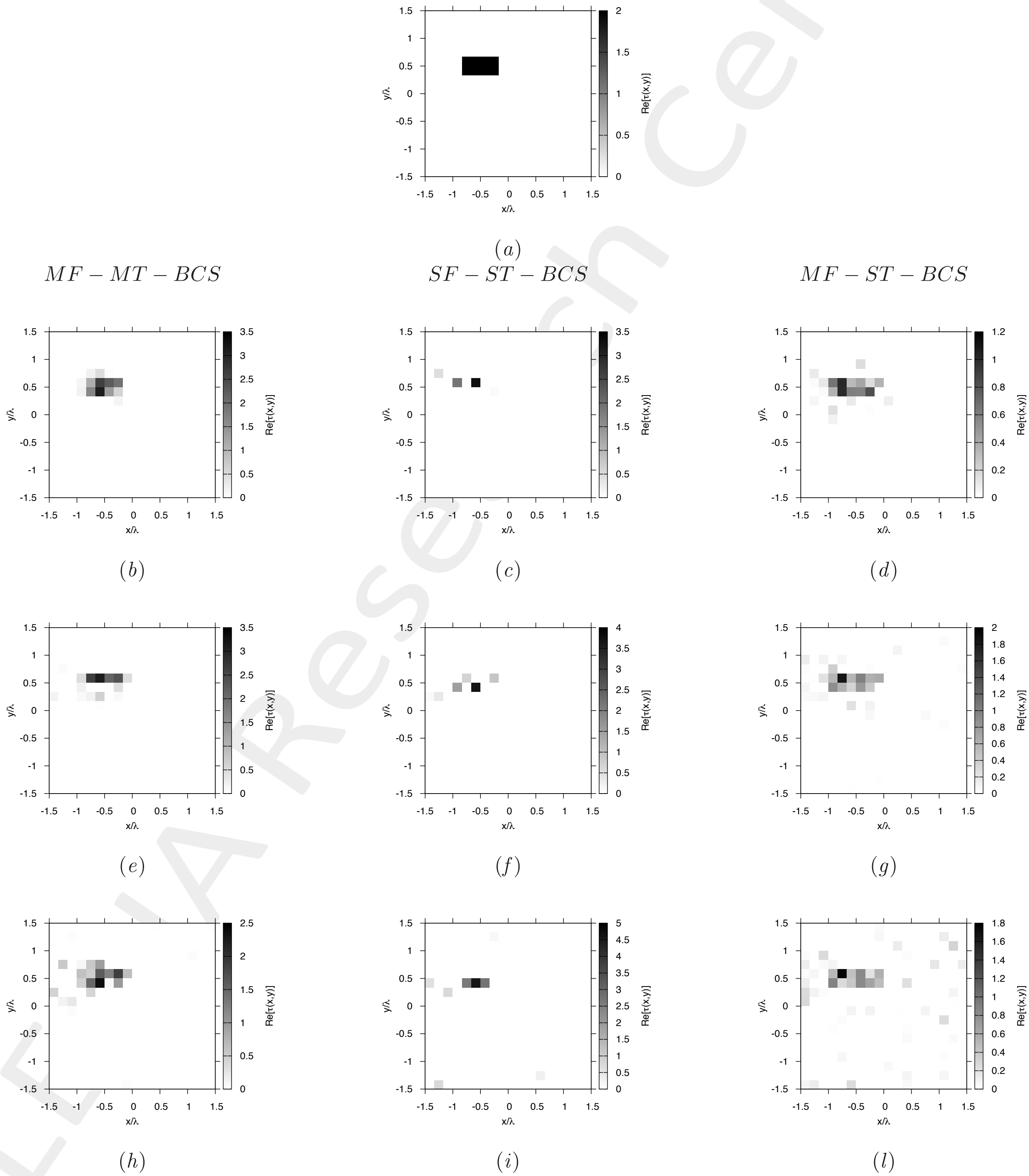

Figure 58. Actual object (a), $MF-MT-BCS$ reconstructed object $(b)(e)(h)$, $SF-ST-BCS$ $(c)(f)(i)$ and $MF-ST-BCS$ $(d)(g)(l)$ for $SNR = 50$ [dB] $(b)(c)(d)$, $SNR = 10$ [dB] $(e)(f)(g)$ and $SNR = 5$ [dB] $(h)(i)(l)$.

Homogeneous Rectangle of Sides $l_1 = 0.66\lambda$, $l_2 = 0.33\lambda$ - BCS Errors vs. ε_r Comparison

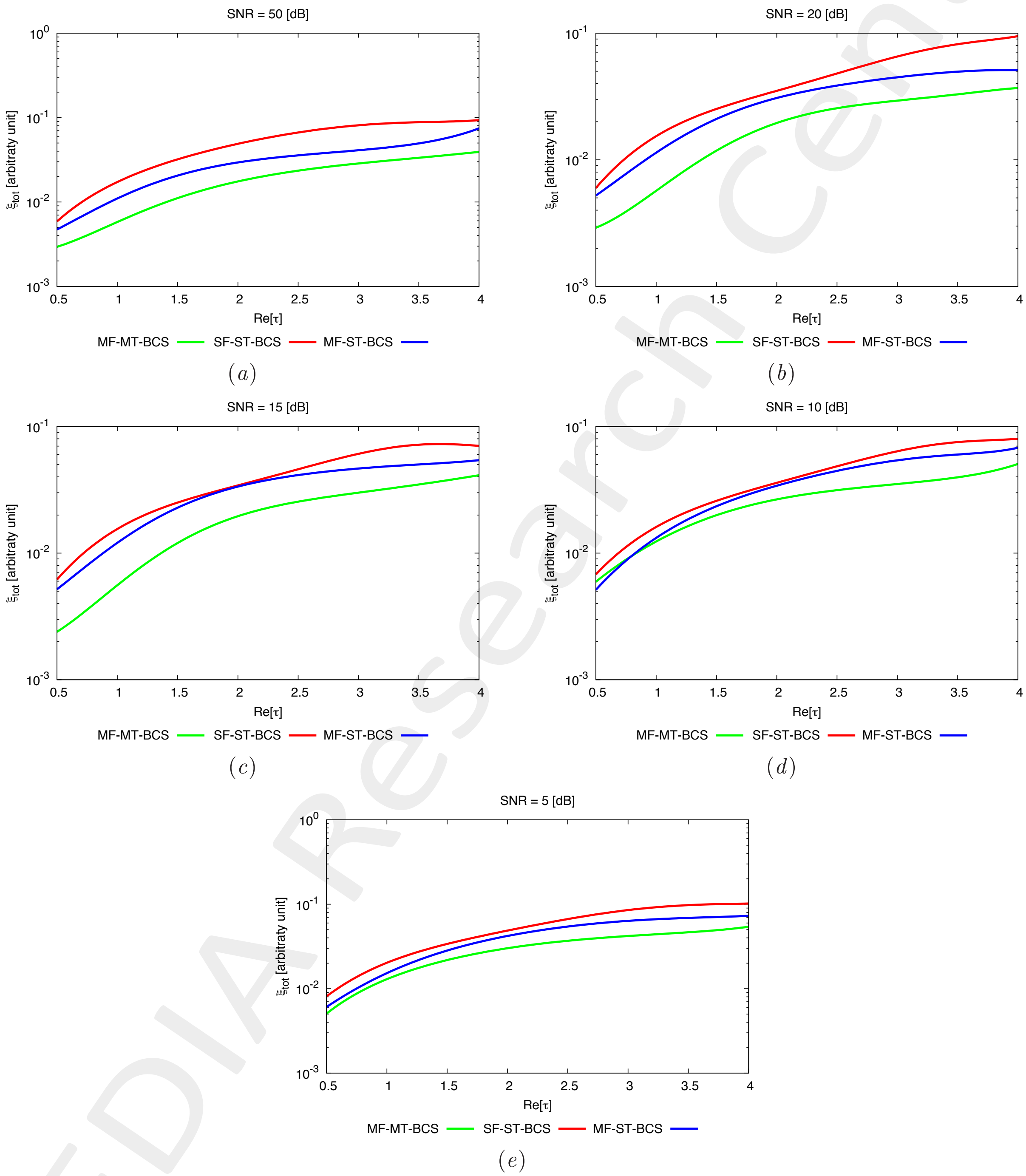

Figure 59. Behaviour of total error ξ_{tot} as a function of ε_r, for $SNR = 50$ [dB] (a), $SNR = 20$ [dB] (b), $SNR = 15$ [dB] (c), $SNR = 10$ [dB] (d) and $SNR = 5$ [dB] (e).

Homogeneous Rectangle of Sides $l_1 = 0.66\lambda$, $l_2 = 0.33\lambda$ - BCS Errors vs. SNR Comparison

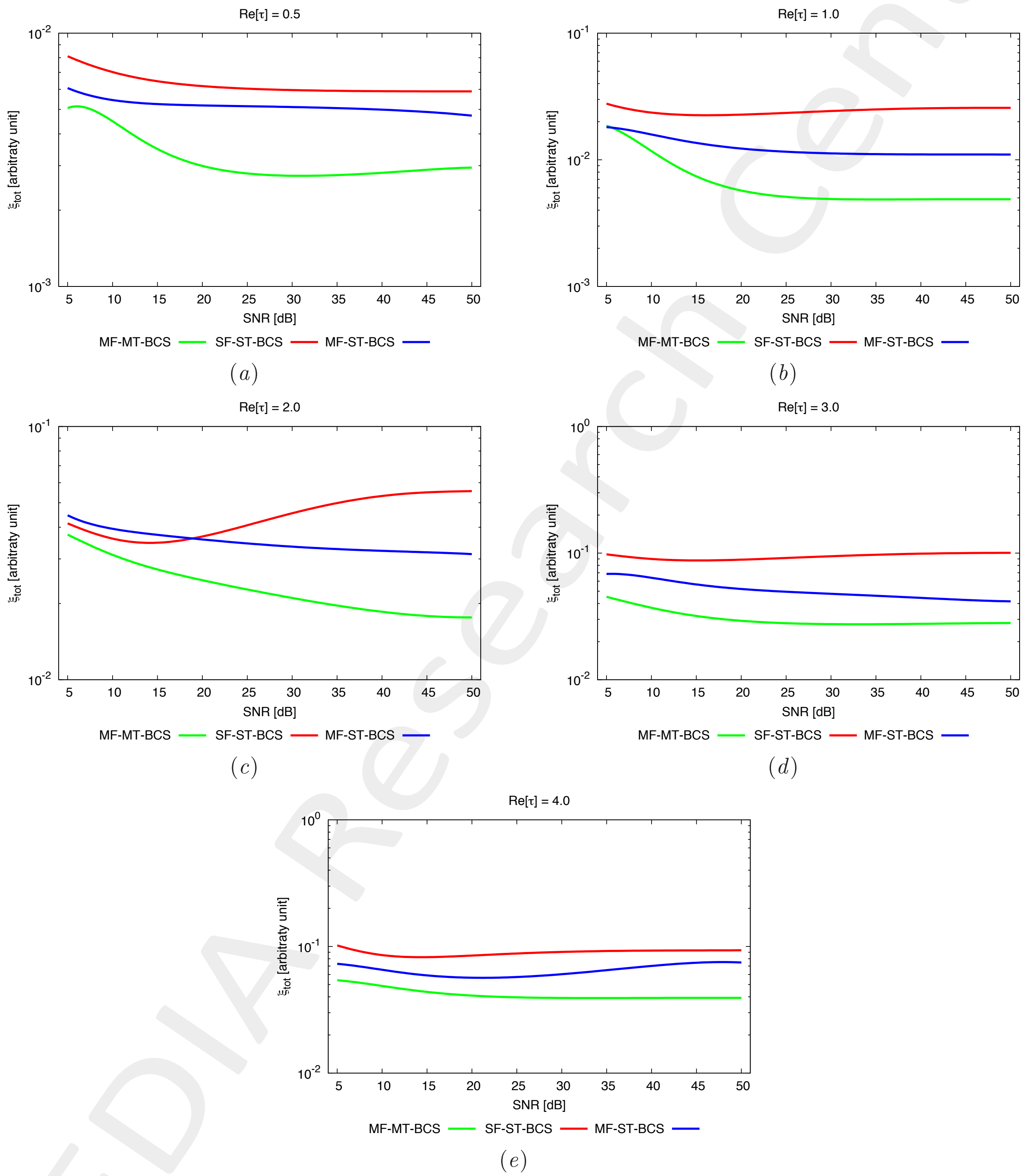

Figure 60. Behaviour of total error ξ_{tot} as a function of SNR, for $\varepsilon_r = 1.5$ [dB] (a), $\varepsilon_r = 2.0$ [dB] (b), $\varepsilon_r = 3.0$ [dB] (c), $\varepsilon_r = 4.0$ [dB] (d) and $\varepsilon_r = 5.0$ [dB] (e).

1.1.4 Rectangle of Sides $l_1 = 0.66\lambda$, $l_2 = 0.33\lambda$ and Square of Side $l_3 = 0.33\lambda$

Goal: show the performances of the multi-frequency $MT - BCS$ when dealing with a sparse scatterer

- Number of frequencies F
- Number of Views: V
- Number of Measurements: M
- Number of Cells for the Inversion: N
- Number of Cells for the Direct solver: D
- Side of the investigation domain: L

Test Case Description

Direct solver:

- Square domain divided in $\sqrt{D} \times \sqrt{D}$ cells
- Domain side: $L = 3\lambda$ (at the central frequency)
- $D = 1296$ (discretization for the direct solver: $< \lambda/10$)

Investigation domain:

- Square domain divided in $\sqrt{N} \times \sqrt{N}$ cells
- $L = 3\lambda$
- $2ka = 2 \times \frac{2\pi}{\lambda} \times \frac{L\sqrt{2}}{2} = 6\pi\sqrt{2} = 26.65$
- $\#DOF = \frac{(2ka)^2}{2} = \frac{(2\times\frac{2\pi}{\lambda}\times\frac{L\sqrt{2}}{2})^2}{2} = 4\pi^2\left(\frac{L}{\lambda}\right)^2 = 4\pi^2 \times 9 \approx 355.3$
- N scelto in modo da essere vicino a $\#DOF$: $N = 324$ (18×18)

Measurement domain:

- Measurement points taken on a circle of radius $\rho = 3\lambda$ (at the central frequency)
- $M \approx 2ka \rightarrow M = 27$

Sources:

- $V = 1$ $(\theta = 0°)$
- Amplitude: $A = 1$ (plane waves)
- Number of Frequencies: $F = 11$
- Frequency Range: $I_F = [150\,Mhz\,:\,450MHz]$ - Frequency Step: $S_F = [30\,Mhz]$

Object:

- Rectangle of sides $l_1^{obj_1} = 0.33\lambda$, $l_2^{obj_1} = 0.66\lambda$; Square of sides $l^{obj_2} = 0.33\lambda$
- $\varepsilon_r = \in \{1.5, 2.0, 2.5, 3.0, 3.5, 4.0, 4.5, 5.0\}$
- $\sigma = 0$ [S/m]

BCS parameters:

- Gamma prior on noise variance parameters: $\beta_1 = 6.5 \times 10^{-1}$, $\beta_2 = 5.8 \times 10^{-2}$
- Convergenze parameter: $\tau = 1.0 \times 10^{-8}$

Homogeneous Rectangle of Sides $l_1^{obj_1} = 0.66\lambda$, $l_2^{obj_1} = 0.33\lambda$ and Square of Side $l^{obj_2} = 0.33\lambda$ - $\varepsilon_r = 1.5$ - BCS Reconstructions Comparison

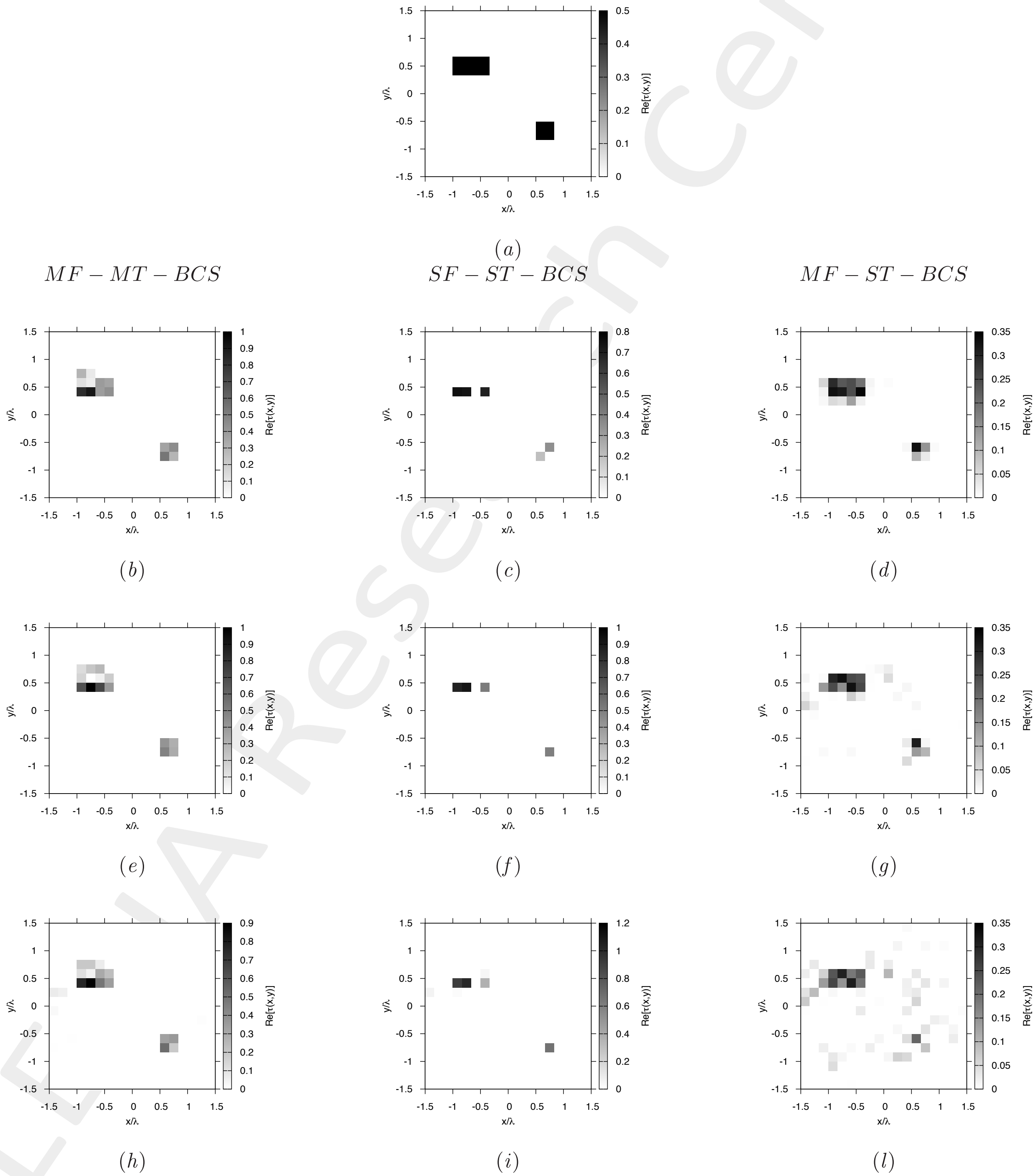

Figure 61. Actual object (a), $MF-MT-BCS$ reconstructed object $(b)(e)(h)$, $SF-ST-BCS$ $(c)(f)(i)$ and $MF-ST-BCS$ $(d)(g)(l)$ for $SNR = 50$ [dB] $(b)(c)(d)$, $SNR = 10$ [dB] $(e)(f)(g)$ and $SNR = 5$ [dB] $(h)(i)(l)$.

Homogeneous Rectangle of Sides $l_1^{obj_1} = 0.66\lambda$, $l_2^{obj_1} = 0.33\lambda$ and Square of Side $l^{obj_2} = 0.33\lambda$ - $\varepsilon_r = 2.0$ - BCS Reconstructions Comparison

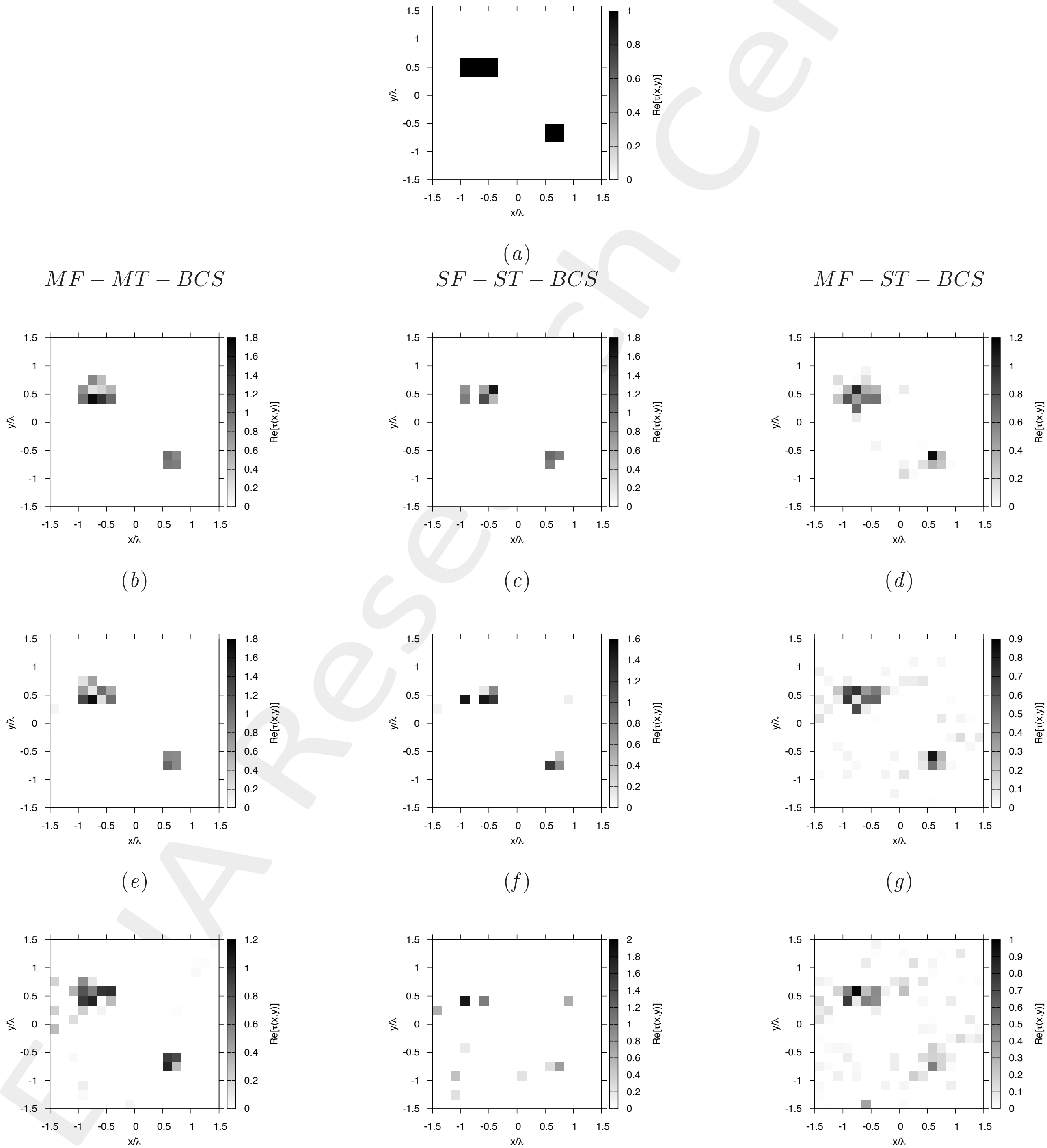

(a)

$MF-MT-BCS$ $SF-ST-BCS$ $MF-ST-BCS$

(b) (c) (d)

(e) (f) (g)

(h) (i) (l)

Figure 62. Actual object (a), $MF-MT-BCS$ reconstructed object $(b)(e)(h)$, $SF-ST-BCS$ $(c)(f)(i)$ and $MF-ST-BCS$ $(d)(g)(l)$ for $SNR = 50$ [dB] $(b)(c)(d)$, $SNR = 10$ [dB] $(e)(f)(g)$ and $SNR = 5$ [dB] $(h)(i)(l)$.

Homogeneous Rectangle of Sides $l_1^{obj_1} = 0.66\lambda$, $l_2^{obj_1} = 0.33\lambda$ and Square of Side $l^{obj_2} = 0.33\lambda$ - $\varepsilon_r = 3.0$ - BCS Reconstructions Comparison

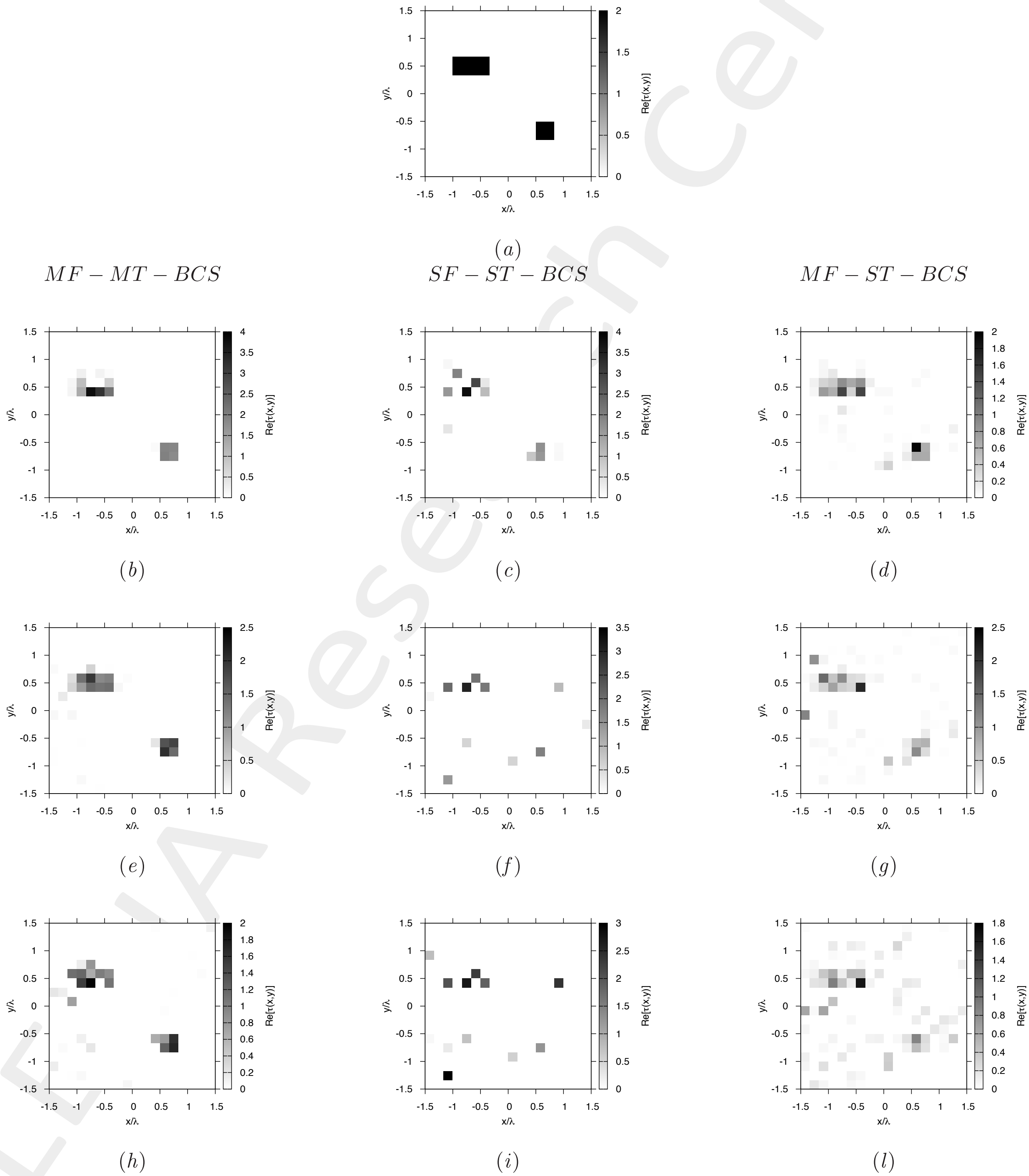

Figure 63. Actual object (a), $MF-MT-BCS$ reconstructed object $(b)(e)(h)$, $SF-ST-BCS$ $(c)(f)(i)$ and $MF-ST-BCS$ $(d)(g)(l)$ for $SNR = 50$ [dB] $(b)(c)(d)$, $SNR = 10$ [dB] $(e)(f)(g)$ and $SNR = 5$ [dB] $(h)(i)(l)$.

Homogeneous Rectangle of Sides $l_1^{obj_1} = 0.66\lambda$, $l_2^{obj_1} = 0.33\lambda$ and Square of Side $l^{obj_2} = 0.33\lambda$ - BCS Errors vs. ε_r Comparison

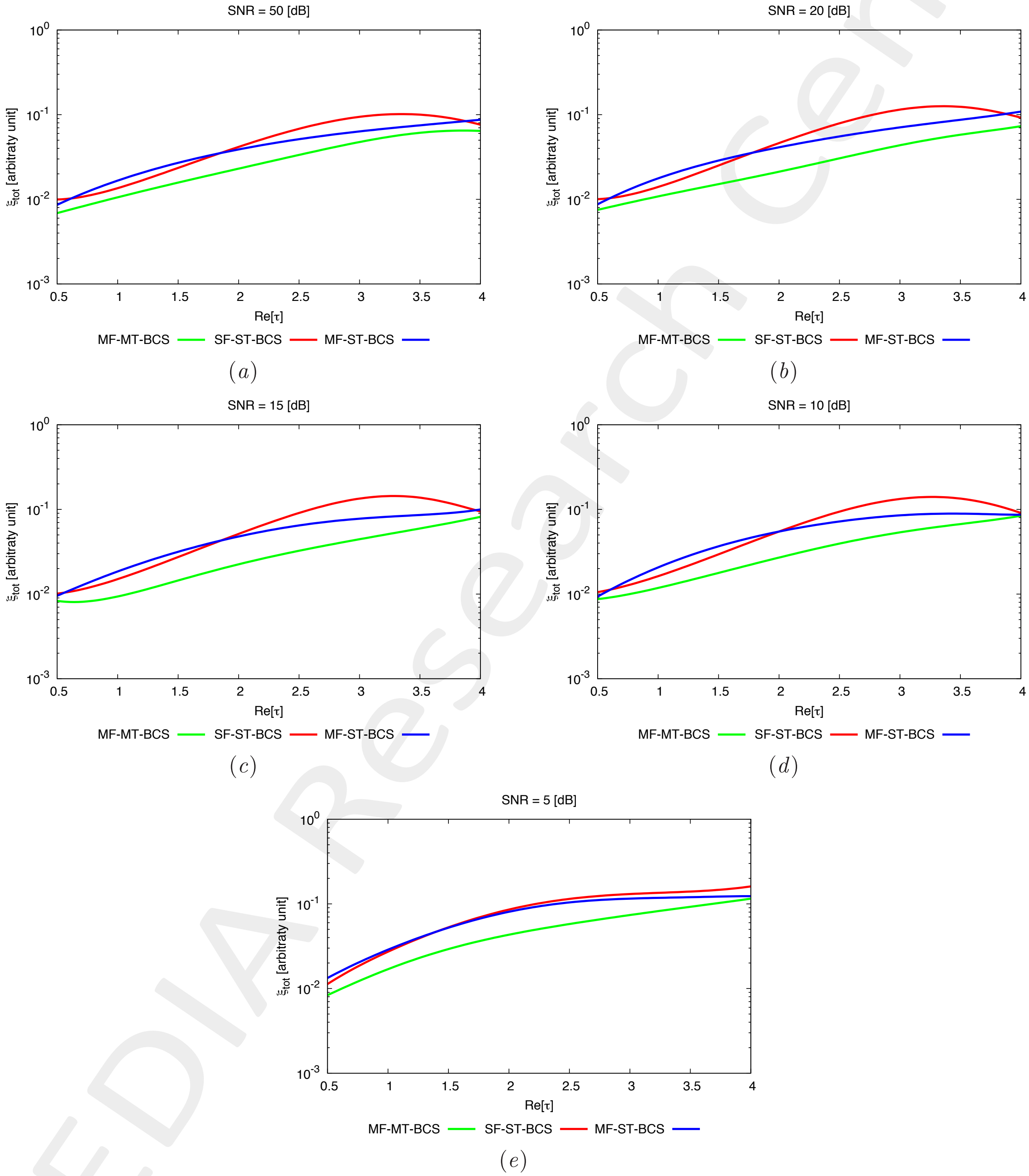

Figure 64. Behaviour of total error ξ_{tot} as a function of ε_r, for $SNR = 50$ [dB] (a), $SNR = 20$ [dB] (b), $SNR = 15$ [dB] (c), $SNR = 10$ [dB] (d) and $SNR = 5$ [dB] (e).

Homogeneous Rectangle of Sides $l_1^{obj_1} = 0.66\lambda$, $l_2^{obj_1} = 0.33\lambda$ and Square of Side $l^{obj_2} = 0.33\lambda$ - BCS Errors vs. SNR Comparison

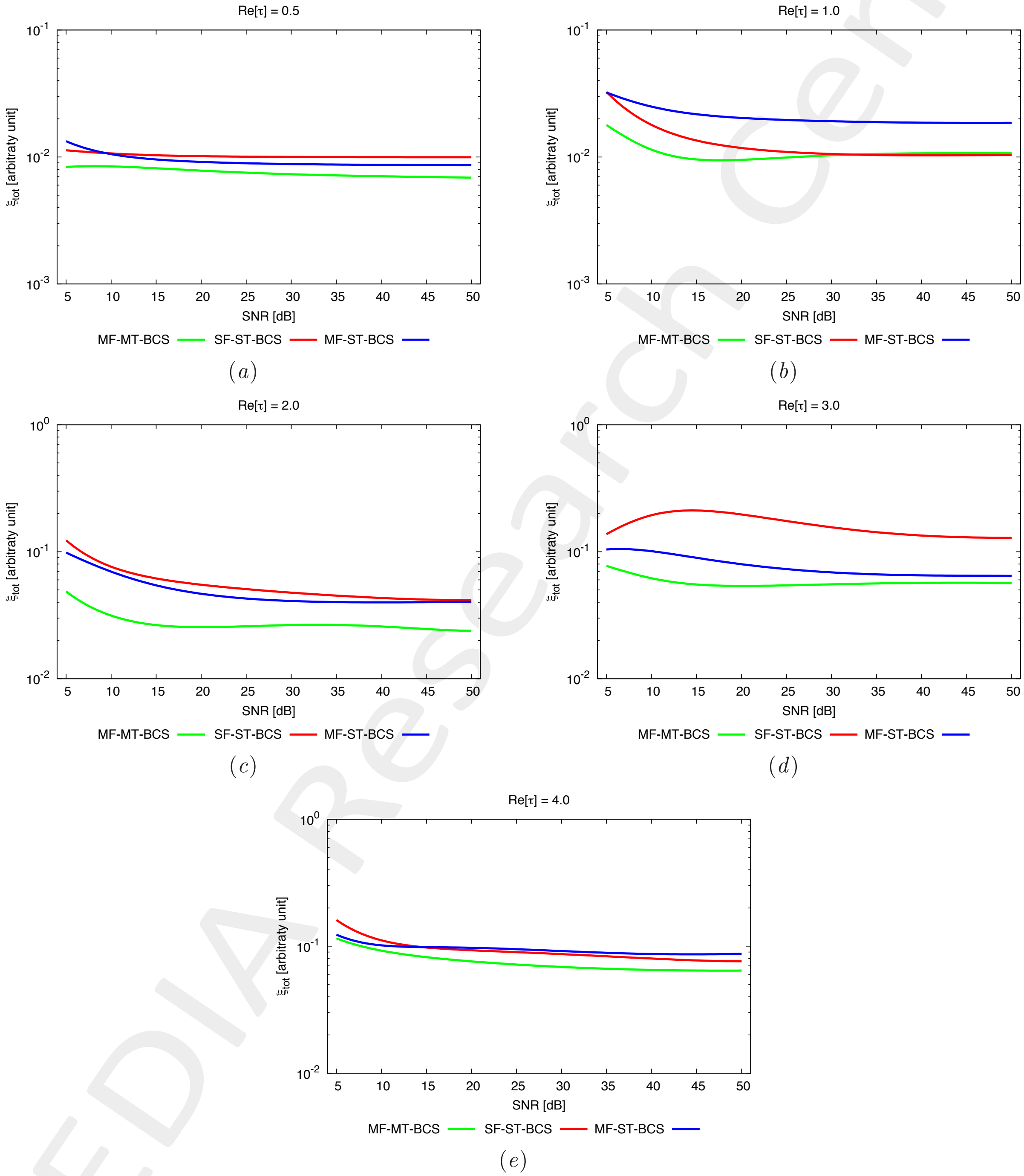

Figure 65. Behaviour of total error ξ_{tot} as a function of SNR, for $\varepsilon_r = 1.5$ [dB] (a), $\varepsilon_r = 2.0$ [dB] (b), $\varepsilon_r = 3.0$ [dB] (c), $\varepsilon_r = 4.0$ [dB] (d) and $\varepsilon_r = 5.0$ [dB] (e).

1.2 Non-Homogeneous Objects

1.2.1 Two Strips of Sides $l_1 = 0.16\lambda$, $l_2 = 0.50\lambda$

Goal: show the performances of the multi-frequency $MT - BCS$ when dealing with a sparse scatterer

- Number of frequencies F
- Number of Views: V
- Number of Measurements: M
- Number of Cells for the Inversion: N
- Number of Cells for the Direct solver: D
- Side of the investigation domain: L

Test Case Description

Direct solver:

- Square domain divided in $\sqrt{D} \times \sqrt{D}$ cells
- Domain side: $L = 3\lambda$ (at the central frequency)
- $D = 1296$ (discretization for the direct solver: $< \lambda/10$)

Investigation domain:

- Square domain divided in $\sqrt{N} \times \sqrt{N}$ cells
- $L = 3\lambda$
- $2ka = 2 \times \frac{2\pi}{\lambda} \times \frac{L\sqrt{2}}{2} = 6\pi\sqrt{2} = 26.65$
- $\#DOF = \frac{(2ka)^2}{2} = \frac{(2\times\frac{2\pi}{\lambda}\times\frac{L\sqrt{2}}{2})^2}{2} = 4\pi^2\left(\frac{L}{\lambda}\right)^2 = 4\pi^2 \times 9 \approx 355.3$
- N scelto in modo da essere vicino a $\#DOF$: $N = 324$ (18×18)

Measurement domain:

- Measurement points taken on a circle of radius $\rho = 3\lambda$ (at the central frequency)
- $M \approx 2ka \rightarrow M = 27$

Sources:

- $V = 1$ $(\theta = 0°)$
- Amplitude: $A = 1$ (plane waves)
- Number of Frequencies: $F = 11$
- Frequency Range: $I_F = [150\,Mhz\,:\,450MHz]$ - Frequency Step: $S_F = [30\,Mhz]$

Object:

- Two strips of sides $l_1 = 0.16\lambda$, $l_2 = 0.50\lambda$
- $\varepsilon_r^{obj_1} \in \{1.5, 2.0, 2.5, 3.0, 3.5, 4.0, 4.5, 5.0\}$, $\varepsilon_r^{obj_2} = 1.6$
- $\sigma = 0$ [S/m]

BCS parameters:

- Gamma prior on noise variance parameter: $\beta_1 = 6.5 \times 10^{-1}$, $\beta_2 = 5.8 \times 10^{-2}$
- Convergenze parameter: $\tau = 1.0 \times 10^{-8}$

Two Non-Homogeneous Strips of Sides $l_1 = 0.16\lambda$, $l_2 = 0.50\lambda$ - $\varepsilon_r = 1.5$ - BCS Reconstructions Comparison

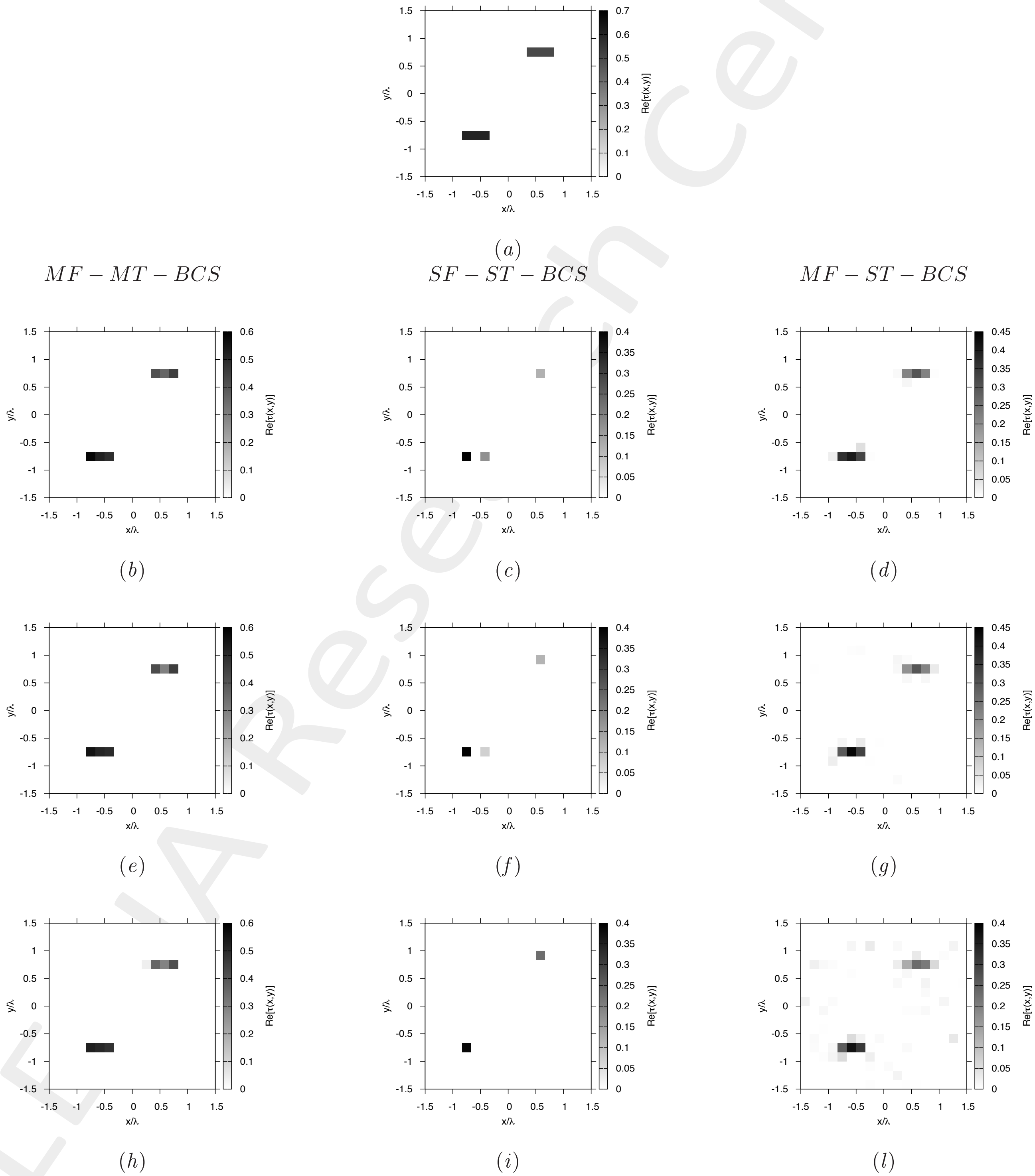

Figure 66. Actual object (a), $MF - MT - BCS$ reconstructed object $(b)(e)(h)$, $SF - ST - BCS$ $(c)(f)(i)$ and $MF - ST - BCS$ $(d)(g)(l)$ for $SNR = 50$ [dB] $(b)(c)(d)$, $SNR = 10$ [dB] $(e)(f)(g)$ and $SNR = 5$ [dB] $(h)(i)(l)$.

Two Non-Homogeneous Strips of Sides $l_1 = 0.16\lambda$, $l_2 = 0.50\lambda$ - $\varepsilon_r = 2.0$ - BCS Reconstructions Comparison

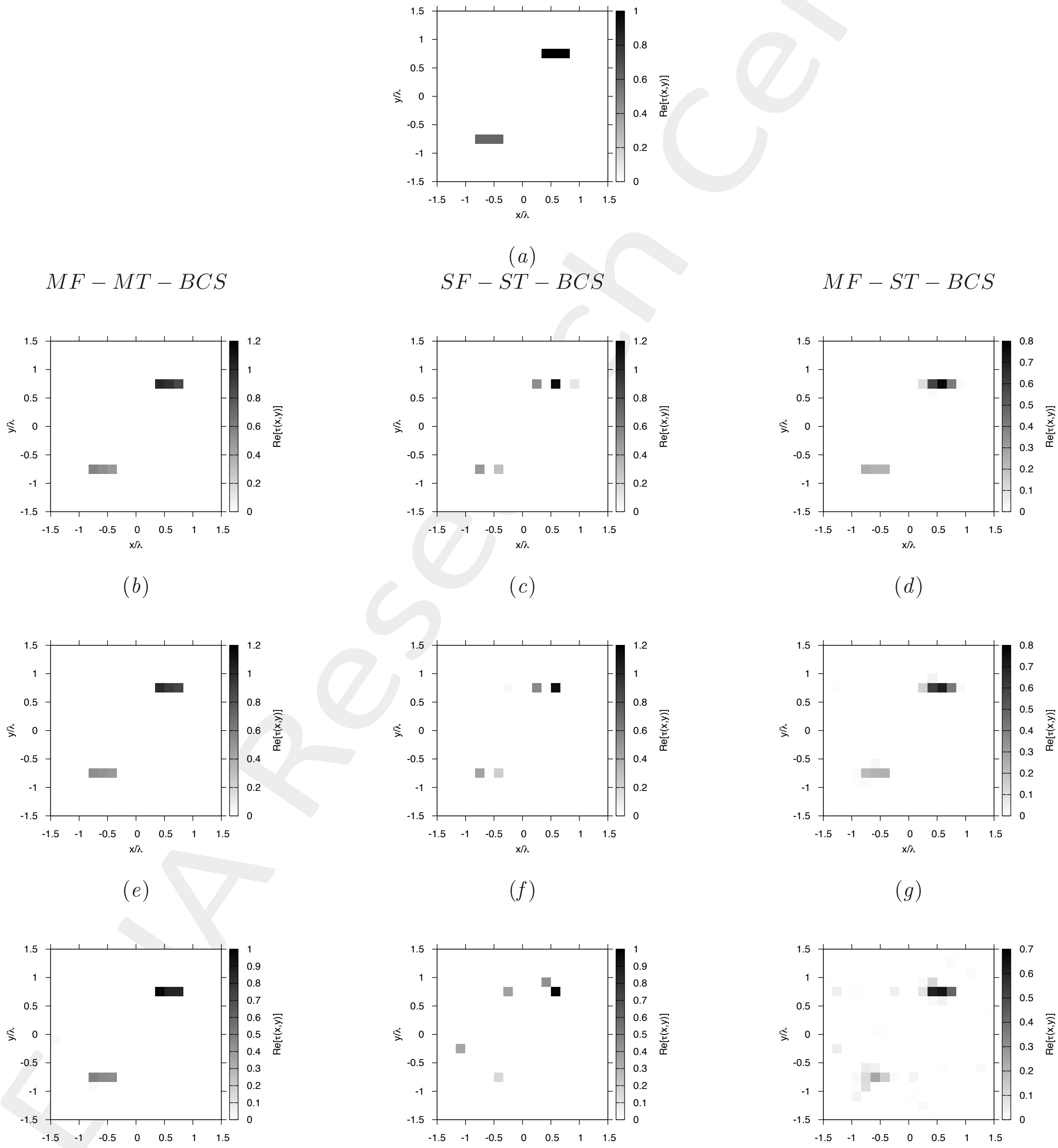

(a)

$MF-MT-BCS$ $SF-ST-BCS$ $MF-ST-BCS$

(b) (c) (d)

(e) (f) (g)

(h) (i) (l)

Figure 67. Actual object (a), $MF-MT-BCS$ reconstructed object $(b)(e)(h)$, $SF-ST-BCS$ $(c)(f)(i)$ and $MF-ST-BCS$ $(d)(g)(l)$ for $SNR=50$ [dB] $(b)(c)(d)$, $SNR=10$ [dB] $(e)(f)(g)$ and $SNR=5$ [dB] $(h)(i)(l)$.

Two Non-Homogeneous Strips of Sides $l_1 = 0.16\lambda$, $l_2 = 0.50\lambda$ - $\varepsilon_r = 3.0$ - BCS Reconstructions Comparison

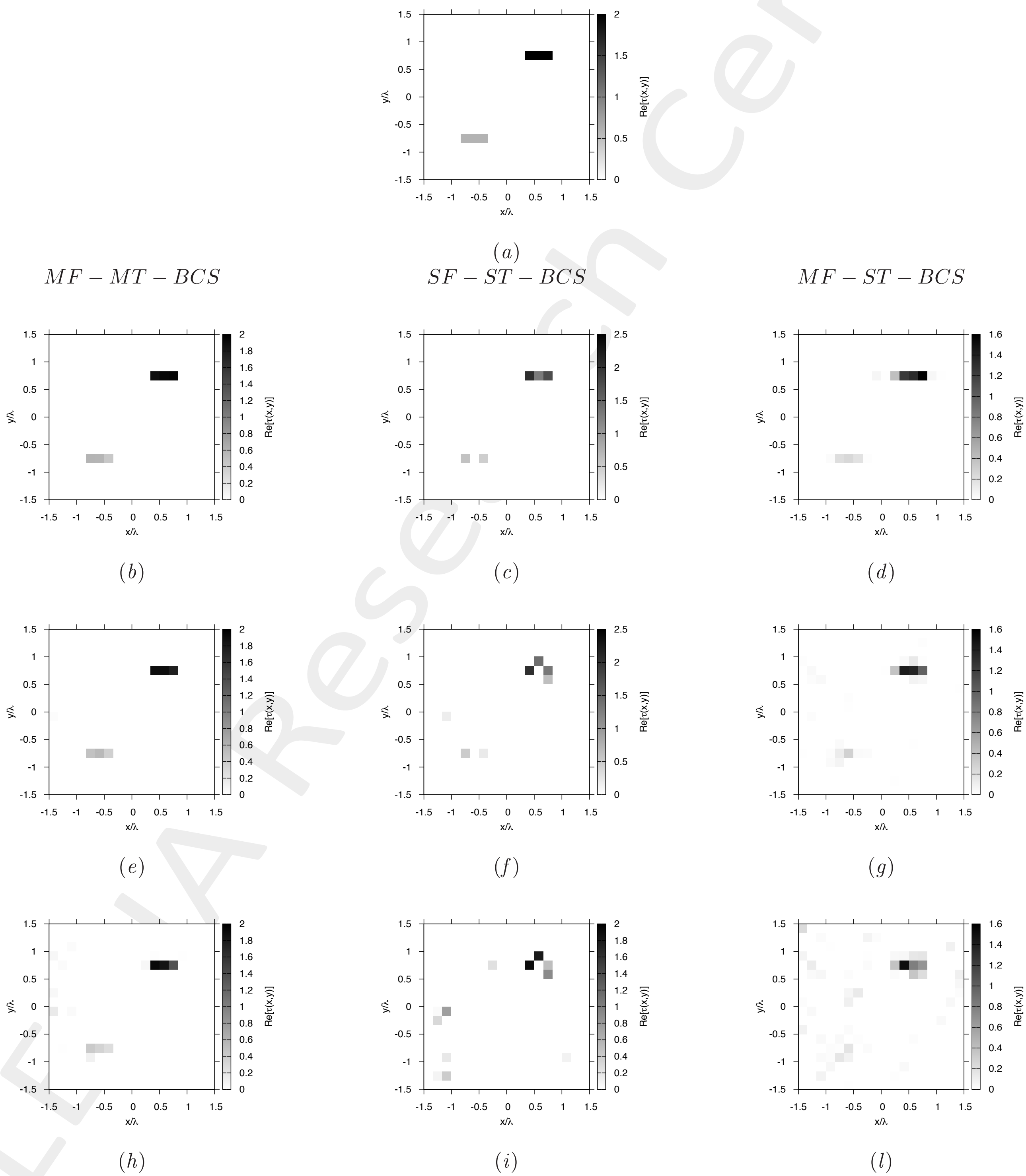

Figure 68. Actual object (a), $MF-MT-BCS$ reconstructed object $(b)(e)(h)$, $SF-ST-BCS$ $(c)(f)(i)$ and $MF-ST-BCS$ $(d)(g)(l)$ for $SNR = 50$ [dB] $(b)(c)(d)$, $SNR = 10$ [dB] $(e)(f)(g)$ and $SNR = 5$ [dB] $(h)(i)(l)$.

Two Non-Homogeneous Strips of Sides $l_1 = 0.16\lambda$, $l_2 = 0.50\lambda$ - $\varepsilon_r = 4.0$ - BCS Reconstructions Comparison

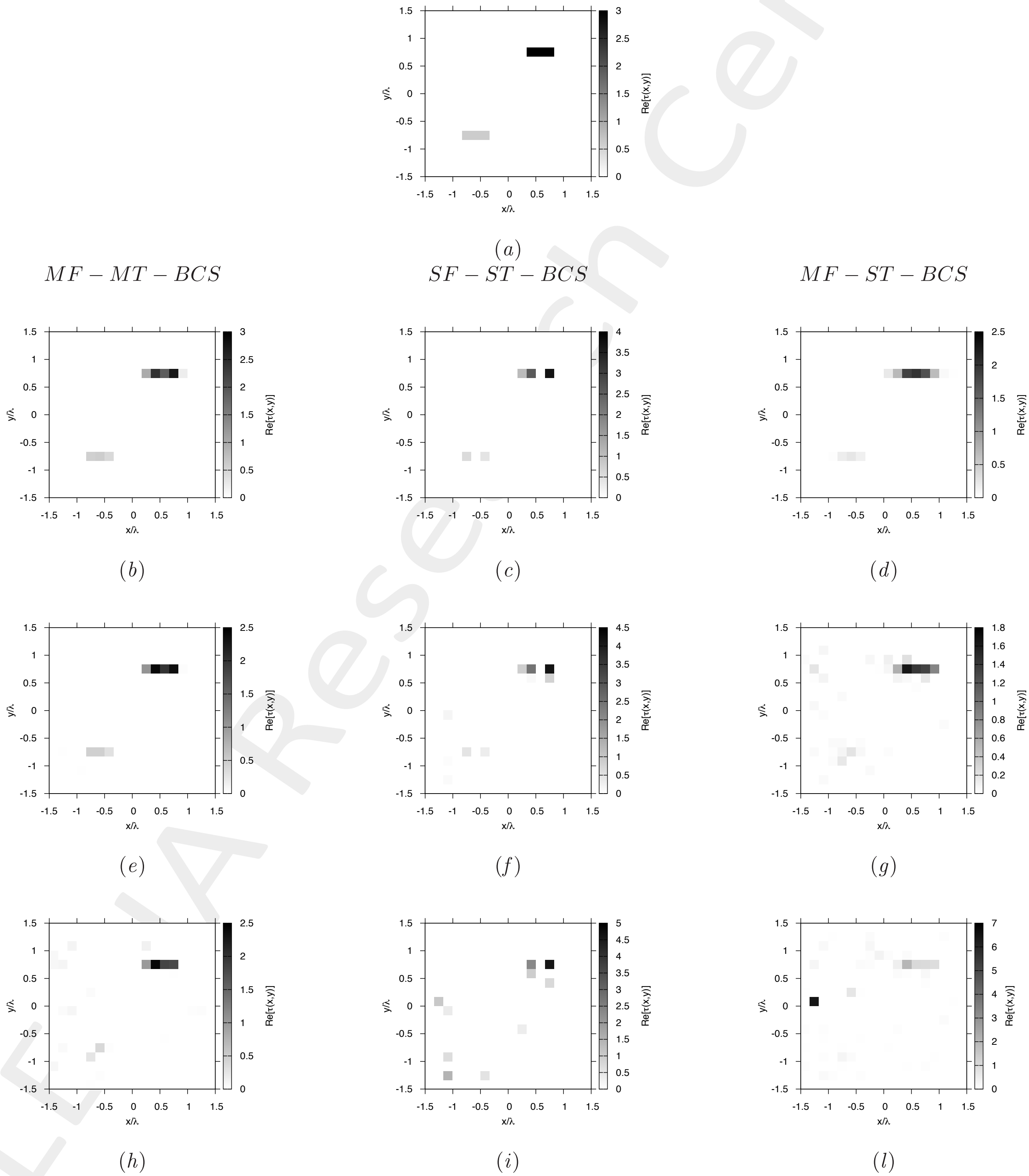

Figure 69. Actual object (a), $MF-MT-BCS$ reconstructed object $(b)(e)(h)$, $SF-ST-BCS$ $(c)(f)(i)$ and $MF-ST-BCS$ $(d)(g)(l)$ for $SNR = 50$ [dB] $(b)(c)(d)$, $SNR = 10$ [dB] $(e)(f)(g)$ and $SNR = 5$ [dB] $(h)(i)(l)$.

Two Non-Homogeneous Strips of Sides $l_1 = 0.16\lambda$, $l_2 = 0.50\lambda$ - $\varepsilon_r = 5.0$ - BCS Reconstructions Comparison

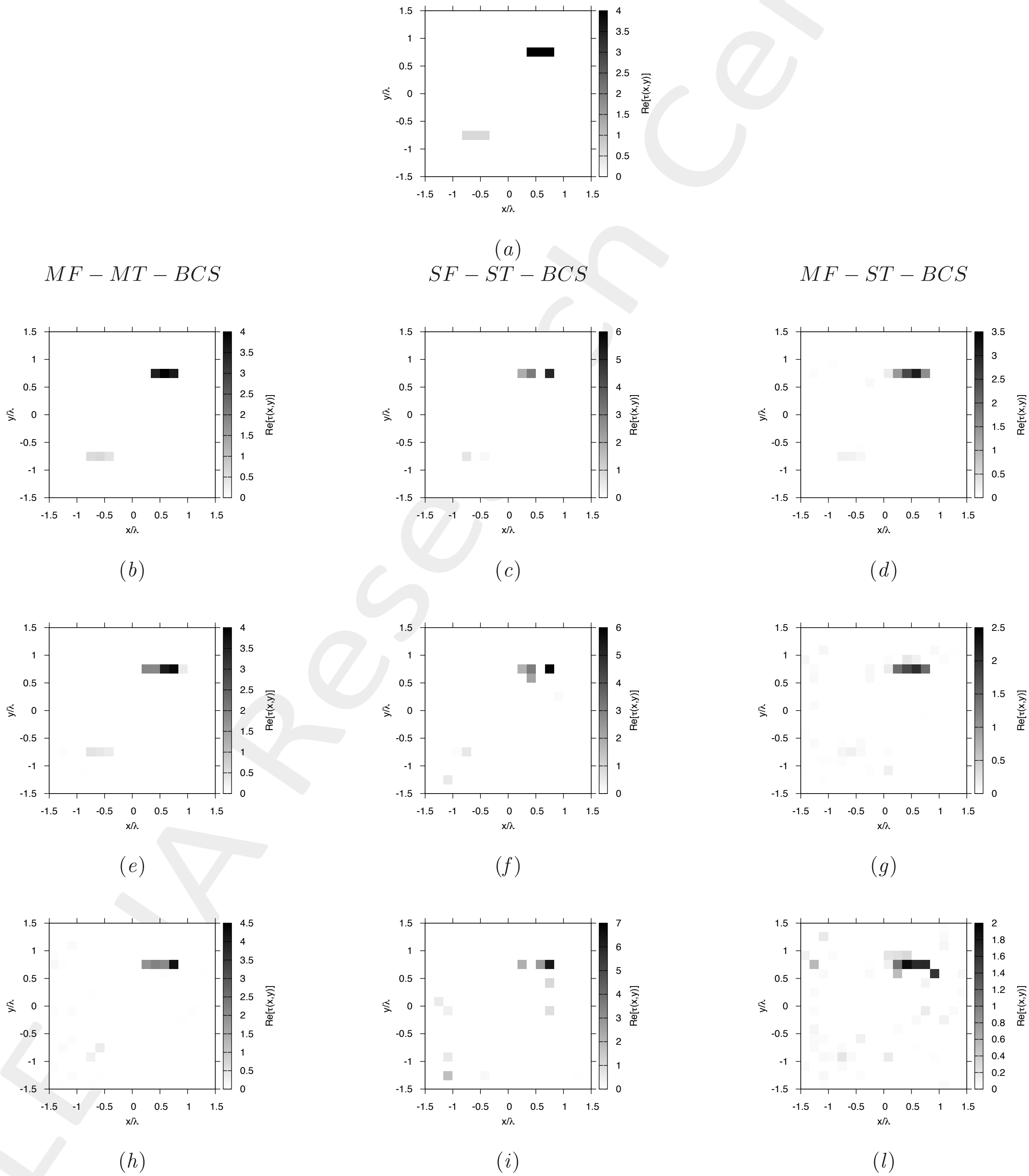

Figure 70. Actual object (a), $MF-MT-BCS$ reconstructed object $(b)(e)(h)$, $SF-ST-BCS$ $(c)(f)(i)$ and $MF-ST-BCS$ $(d)(g)(l)$ for $SNR = 50$ [dB] $(b)(c)(d)$, $SNR = 10$ [dB] $(e)(f)(g)$ and $SNR = 5$ [dB] $(h)(i)(l)$.

Two Non-Homogeneous Strips of Sides $l_1 = 0.16\lambda$, $l_2 = 0.50\lambda$ - BCS Errors vs. ε_r Comparison

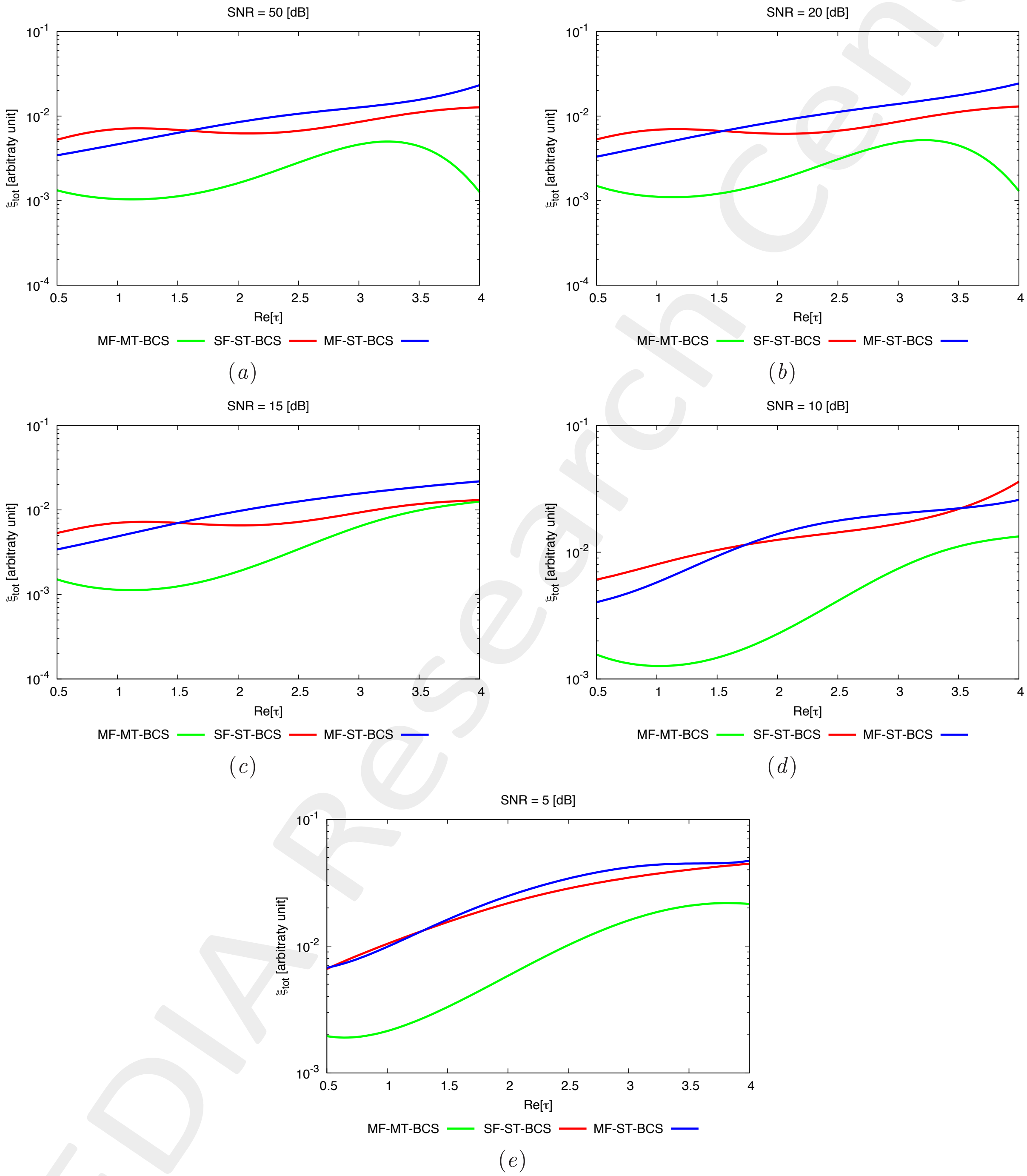

Figure 71. Behaviour of total error ξ_{tot} as a function of ε_r, for $SNR = 50$ [dB] (a), $SNR = 20$ [dB] (b), $SNR = 15$ [dB] (c), $SNR = 10$ [dB] (d) and $SNR = 5$ [dB] (e).

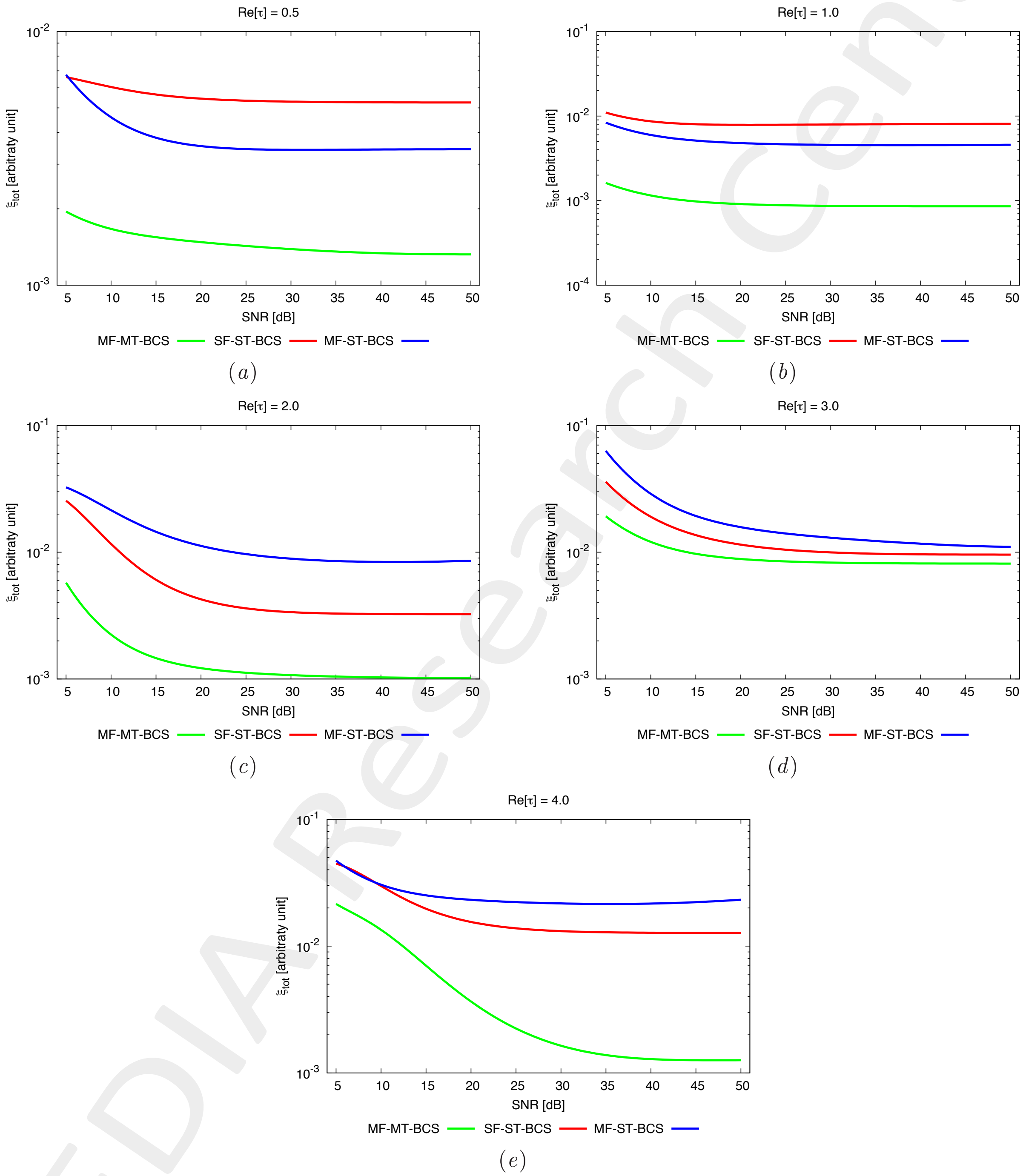

Figure 72. Behaviour of total error ξ_{tot} as a function of SNR, for $\varepsilon_r = 1.5$ [dB] (a), $\varepsilon_r = 2.0$ [dB] (b), $\varepsilon_r = 3.0$ [dB] (c), $\varepsilon_r = 4.0$ [dB] (d) and $\varepsilon_r = 5.0$ [dB] (e).

1.2.2 Rectangle of Sides $l_1 = 0.66\lambda$, $l_2 = 0.33\lambda$ and Square of Side $l_3 = 0.33\lambda$

Goal: show the performances of the multi-frequency $MT - BCS$ when dealing with a sparse scatterer

- Number of frequencies F
- Number of Views: V
- Number of Measurements: M
- Number of Cells for the Inversion: N
- Number of Cells for the Direct solver: D
- Side of the investigation domain: L

Test Case Description

Direct solver:

- Square domain divided in $\sqrt{D} \times \sqrt{D}$ cells
- Domain side: $L = 3\lambda$ (at the central frequency)
- $D = 1296$ (discretization for the direct solver: $< \lambda/10$)

Investigation domain:

- Square domain divided in $\sqrt{N} \times \sqrt{N}$ cells
- $L = 3\lambda$
- $2ka = 2 \times \frac{2\pi}{\lambda} \times \frac{L\sqrt{2}}{2} = 6\pi\sqrt{2} = 26.65$
- $\#DOF = \frac{(2ka)^2}{2} = \frac{(2\times\frac{2\pi}{\lambda}\times\frac{L\sqrt{2}}{2})^2}{2} = 4\pi^2\left(\frac{L}{\lambda}\right)^2 = 4\pi^2 \times 9 \approx 355.3$
- N scelto in modo da essere vicino a $\#DOF$: $N = 324$ (18×18)

Measurement domain:

- Measurement points taken on a circle of radius $\rho = 3\lambda$ (at the central frequency)
- $M \approx 2ka \rightarrow M = 27$

Sources:

- $V = 1$ $(\theta = 0°)$
- Amplitude: $A = 1$ (plane waves)
- Number of Frequencies: $F = 11$
- Frequency Range: $I_F = [150\, Mhz\, :\, 450 MHz]$ - Frequency Step: $S_F = [30\, Mhz]$

Object:

- Rectangle of sides $l_1^{obj_1} = 0.33\lambda$, $l_2^{obj_1} = 0.66\lambda$; Square of sides $l^{obj_2} = 0.33\lambda$
- $\varepsilon_r^{obj_1} = 1.9$, $\varepsilon_r^{obj_2} \in \{1.5, 2.0, 2.5, 3.0, 3.5, 4.0, 4.5, 5.0\}$
- $\sigma = 0$ [S/m]

MT-BCS parameters:

- Gamma prior on noise variance parameters: $\beta_1 = 6.5 \times 10^{-1}$, $\beta_2 = 5.8 \times 10^{-2}$
- Convergenze parameter: $\tau = 1.0 \times 10^{-8}$

Homogeneous Rectangle of Sides $l_1^{obj_1} = 0.66\lambda$, $l_2^{obj_1} = 0.33\lambda$ and Square of Side $l^{obj_2} = 0.33\lambda$ - $\varepsilon_r = 1.5$ - BCS Reconstructions Comparison

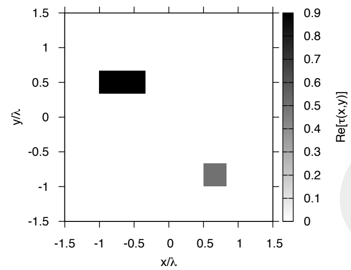

(a)

$MF - MT - BCS$ $\quad$ $SF - ST - BCS$ $\quad$ $MF - ST - BCS$

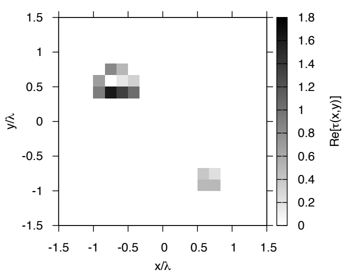

(b)

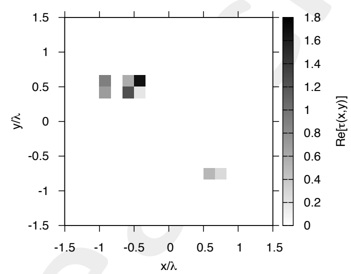

(c)

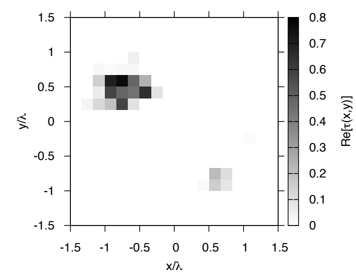

(d)

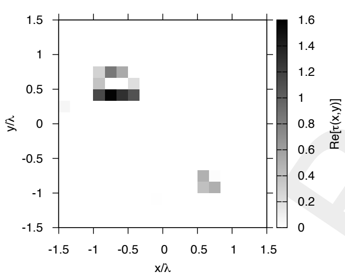

(e)

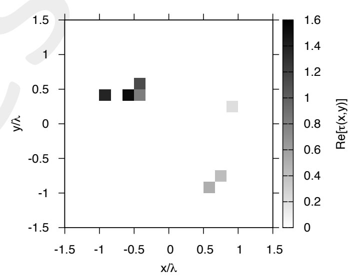

(f)

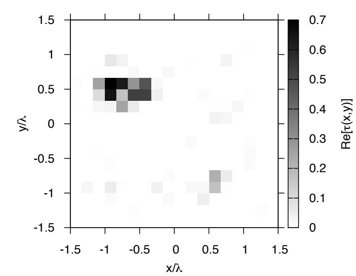

(g)

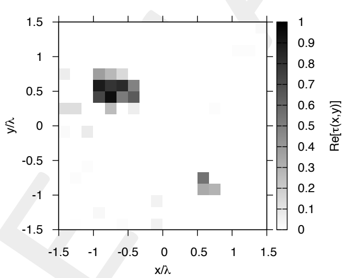

(h)

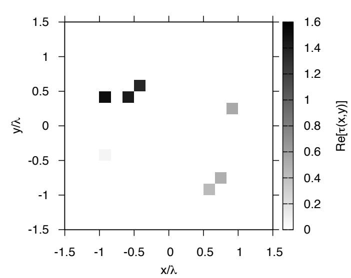

(i)

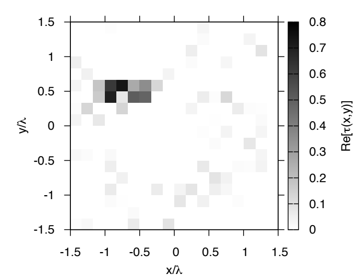

(l)

Figure 80. Actual object (a), $MF - MT - BCS$ reconstructed object $(b)(e)(h)$, $SF - ST - BCS$ $(c)(f)(i)$ and $MF - ST - BCS$ $(d)(g)(l)$ for $SNR = 50$ [dB] $(b)(c)(d)$, $SNR = 10$ [dB] $(e)(f)(g)$ and $SNR = 5$ [dB] $(h)(i)(l)$.

Homogeneous Rectangle of Sides $l_1^{obj_1} = 0.66\lambda$, $l_2^{obj_1} = 0.33\lambda$ and Square of Side $l^{obj_2} = 0.33\lambda$ - $\varepsilon_r = 2.0$ - BCS Reconstructions Comparison

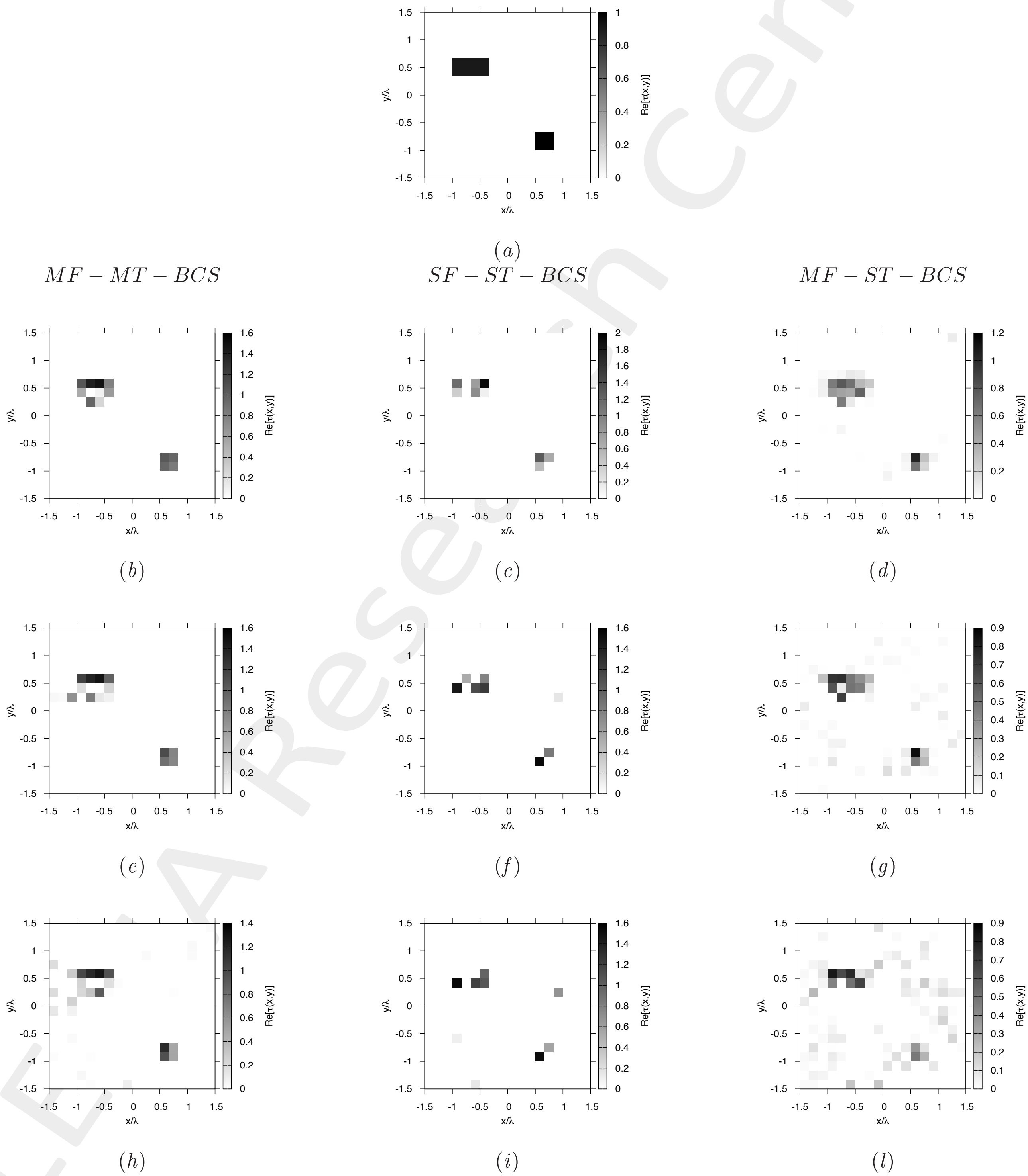

Figure 81. Actual object (a), $MF - MT - BCS$ reconstructed object $(b)(e)(h)$, $SF - ST - BCS$ $(c)(f)(i)$ and $MF - ST - BCS$ $(d)(g)(l)$ for $SNR = 50$ [dB] $(b)(c)(d)$, $SNR = 10$ [dB] $(e)(f)(g)$ and $SNR = 5$ [dB] $(h)(i)(l)$.

Homogeneous Rectangle of Sides $l_1^{obj_1} = 0.66\lambda$, $l_2^{obj_1} = 0.33\lambda$ and Square of Side $l^{obj_2} = 0.33\lambda$ - $\varepsilon_r = 3.0$ - BCS Reconstructions Comparison

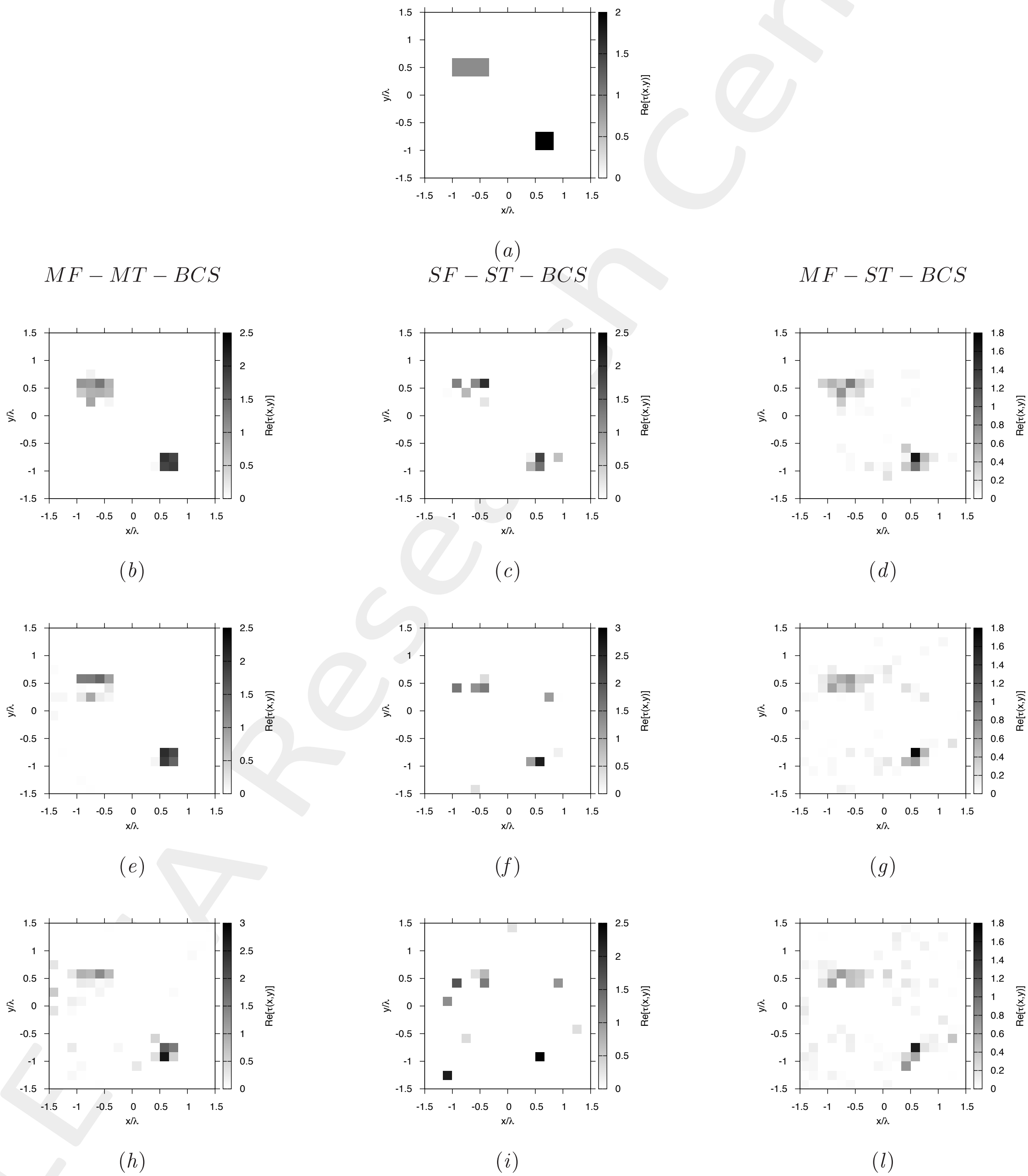

Figure 82. Actual object (a), $MF-MT-BCS$ reconstructed object $(b)(e)(h)$, $SF-ST-BCS$ $(c)(f)(i)$ and $MF-ST-BCS$ $(d)(g)(l)$ for $SNR = 50$ [dB] $(b)(c)(d)$, $SNR = 10$ [dB] $(e)(f)(g)$ and $SNR = 5$ [dB] $(h)(i)(l)$.

Homogeneous Rectangle of Sides $l_1^{obj_1} = 0.66\lambda$, $l_2^{obj_1} = 0.33\lambda$ and Square of Side $l^{obj_2} = 0.33\lambda$ - $\varepsilon_r = 4.0$ - BCS Reconstructions Comparison

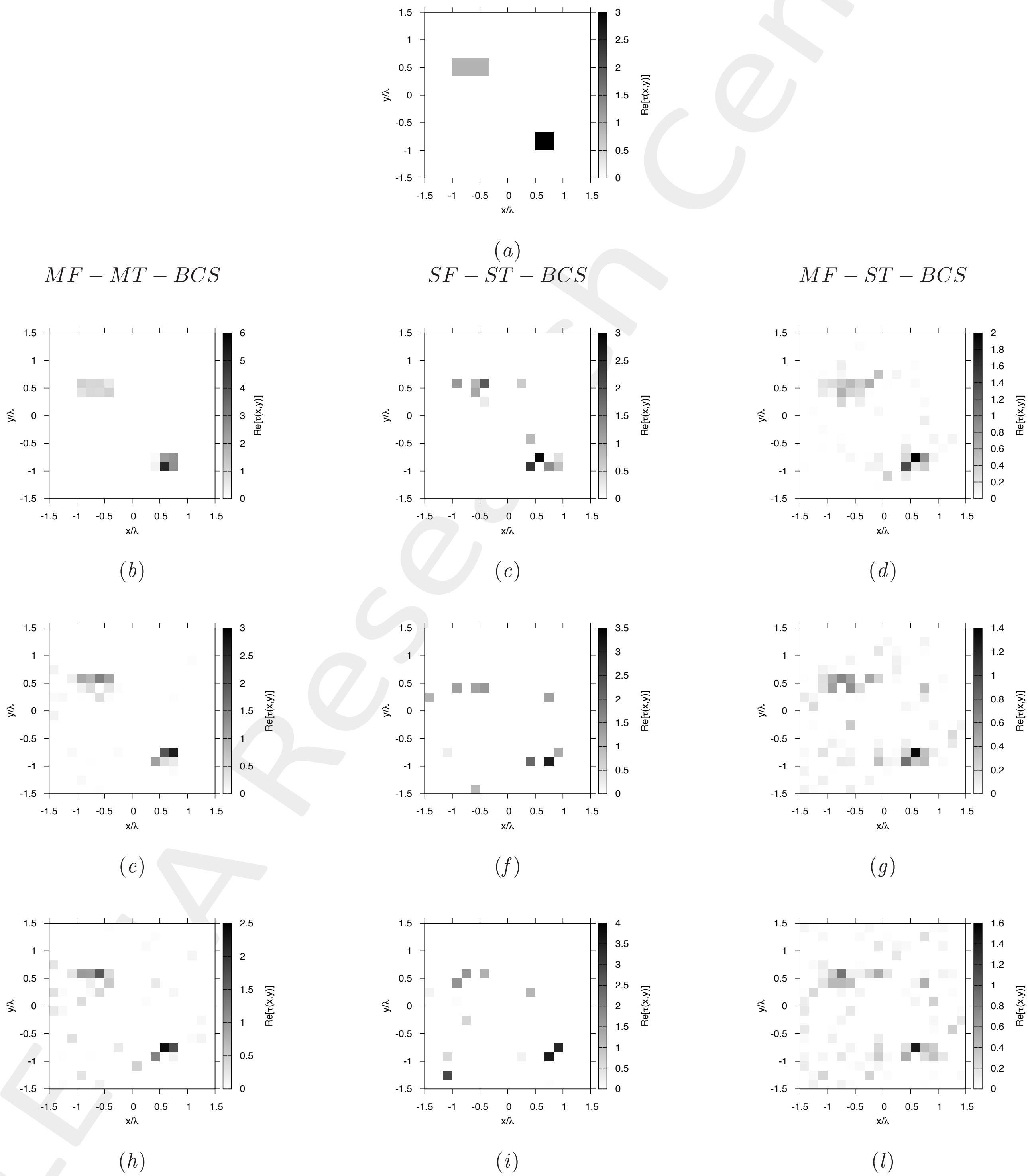

Figure 83. Actual object (a), $MF-MT-BCS$ reconstructed object $(b)(e)(h)$, $SF-ST-BCS$ $(c)(f)(i)$ and $MF-ST-BCS$ $(d)(g)(l)$ for $SNR = 50$ [dB] $(b)(c)(d)$, $SNR = 10$ [dB] $(e)(f)(g)$ and $SNR = 5$ [dB] $(h)(i)(l)$.

Homogeneous Rectangle of Sides $l_1^{obj_1} = 0.66\lambda$, $l_2^{obj_1} = 0.33\lambda$ and Square of Side $l^{obj_2} = 0.33\lambda$ - $\varepsilon_r = 5.0$ - BCS Reconstructions Comparison

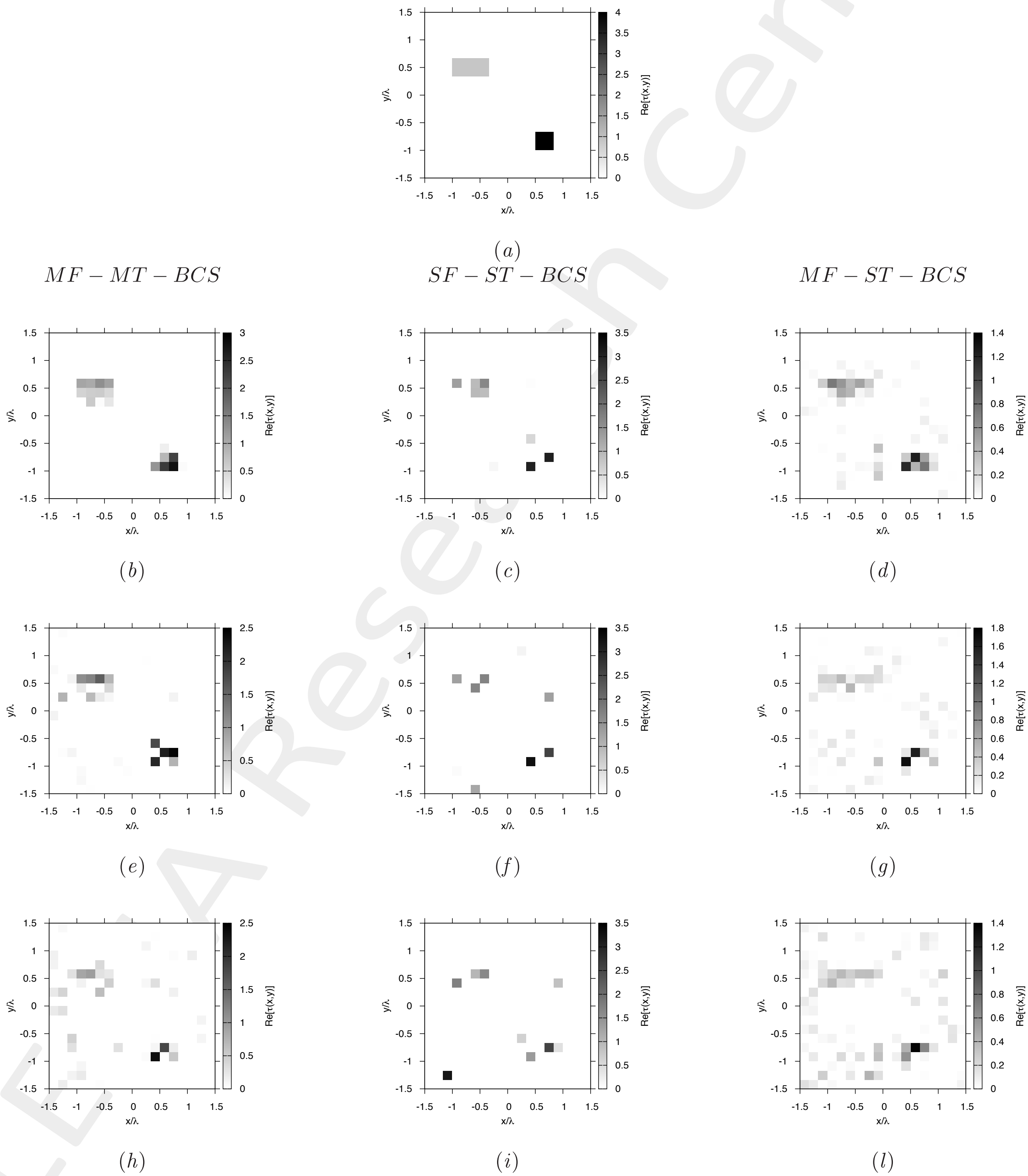

Figure 84. Actual object (a), $MF - MT - BCS$ reconstructed object $(b)(e)(h)$, $SF - ST - BCS$ $(c)(f)(i)$ and $MF - ST - BCS$ $(d)(g)(l)$ for $SNR = 50$ [dB] $(b)(c)(d)$, $SNR = 10$ [dB] $(e)(f)(g)$ and $SNR = 5$ [dB] $(h)(i)(l)$.

Homogeneous Rectangle of Sides $l_1^{obj_1} = 0.66\lambda$, $l_2^{obj_1} = 0.33\lambda$ and Square of Side $l^{obj_2} = 0.33\lambda$ - BCS Errors vs. ε_r Comparison

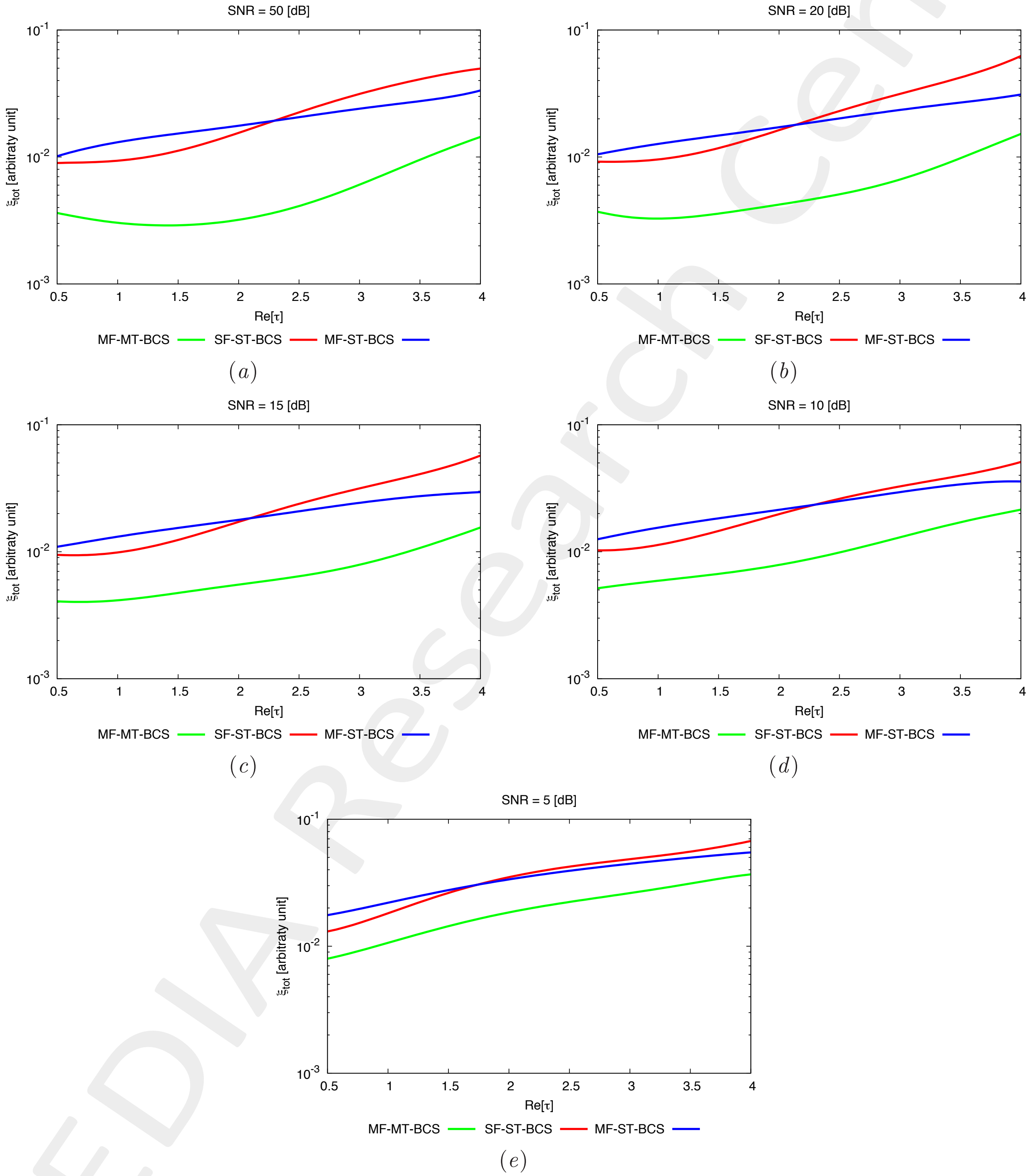

Figure 85. Behaviour of total error ξ_{tot} as a function of ε_r, for $SNR = 50$ [dB] (a), $SNR = 20$ [dB] (b), $SNR = 15$ [dB] (c), $SNR = 10$ [dB] (d) and $SNR = 5$ [dB] (e).

Homogeneous Rectangle of Sides $l_1^{obj_1} = 0.66\lambda$, $l_2^{obj_1} = 0.33\lambda$ and Square of Side $l^{obj_2} = 0.33\lambda$ - BCS Errors vs. SNR Comparison

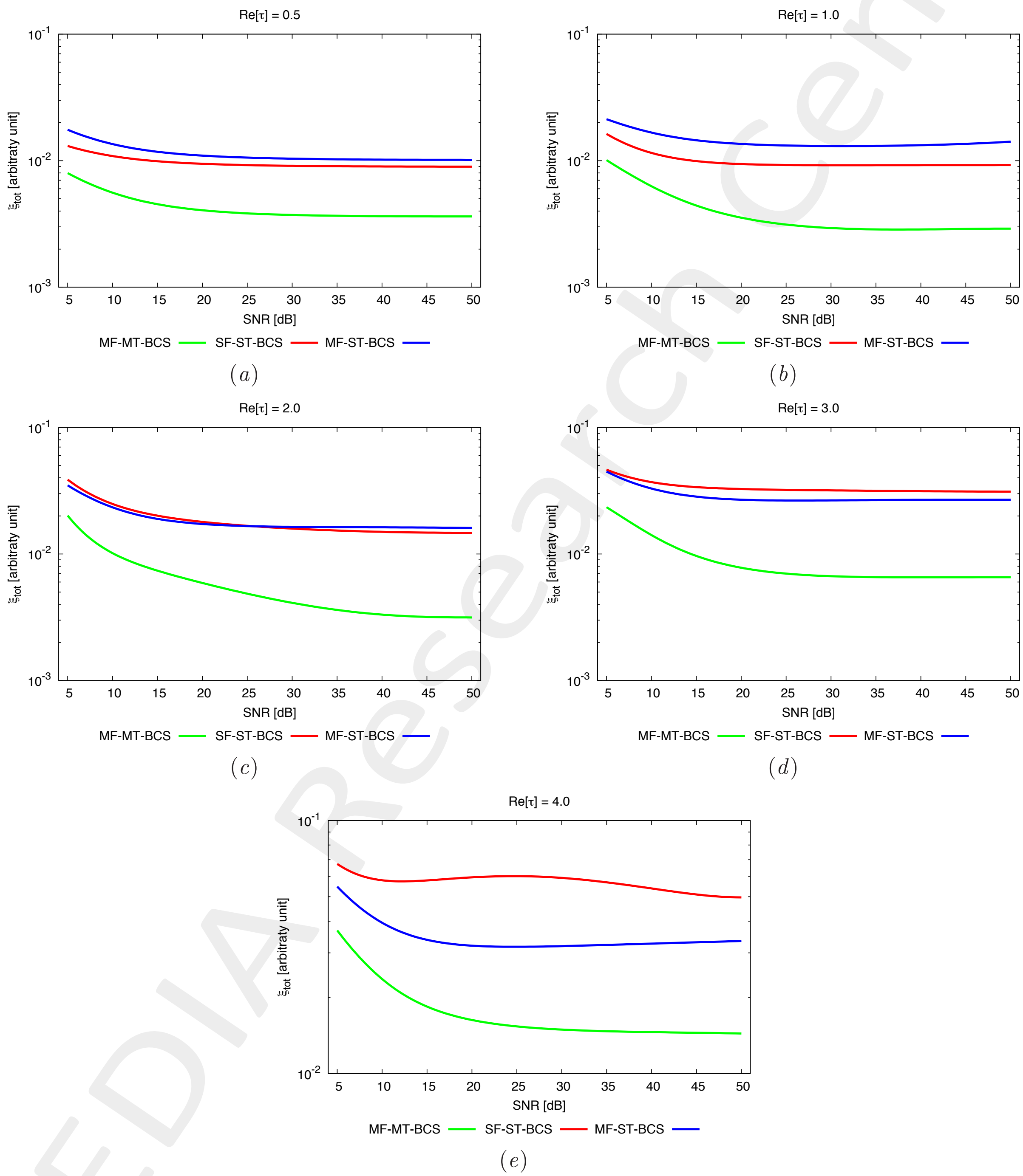

Figure 86. Behaviour of total error ξ_{tot} as a function of SNR, for $\varepsilon_r = 1.5$ [dB] (a), $\varepsilon_r = 2.0$ [dB] (b), $\varepsilon_r = 3.0$ [dB] (c), $\varepsilon_r = 4.0$ [dB] (d) and $\varepsilon_r = 5.0$ [dB] (e).

1.3 Statistical Analysis - Square Cylinders of Side $l = 0.16\lambda$

Goal: show the statistical performances of the multi-frequency $MT - BCS$ when dealing with sparse scatterers

- Number of frequencies F
- Number of Views: V
- Number of Measurements: M
- Number of Cells for the Inversion: N
- Number of Cells for the Direct solver: D
- Side of the investigation domain: L

Test Case Description

Direct solver:

- Square domain divided in $\sqrt{D} \times \sqrt{D}$ cells
- Domain side: $L = 3\lambda$ (at the central frequency)
- $D = 1296$ (discretization for the direct solver: $< \lambda/10$)

Investigation domain:

- Square domain divided in $\sqrt{N} \times \sqrt{N}$ cells
- $L = 3\lambda$
- $N = 324$

Measurement domain:

- Measurement points taken on a circle of radius $\rho = 3\lambda$ (at the central frequency)
- $M \approx 2ka \rightarrow M = 27$

Sources:

- $V \approx 2ka \rightarrow V = 27$
- Amplitude $A = 1$ (plane waves)
- Number of Frequencies: $F = 11$
- Frequency Range: $I_F = [150\,Mhz\ :\ 450MHz]$ - Frequency Step: $S_F = [30\,Mhz]$

Object:

- $S \in \{1, 2, 3, 4, 5, 6, 7, 8, 9, 10\}$ Square cylinders of side $\frac{\lambda}{6} = 0.16667$
- $\varepsilon_r = 2.0$
- $\sigma = 0$ [S/m]

MT-BCS parameters:

- Gamma prior on noise variance parameters: $\beta_1 = 6.5 \times 10^{-1}$, $\beta_2 = 5.8 \times 10^{-2}$
- Convergenze parameter: $\tau = 1.0 \times 10^{-8}$

Statistical Analysis:

- $K = 14$ random seeds used for each case

Statistical Analysis - Error Figures - BCS Comparison - $SNR = 50$ **[dB]**

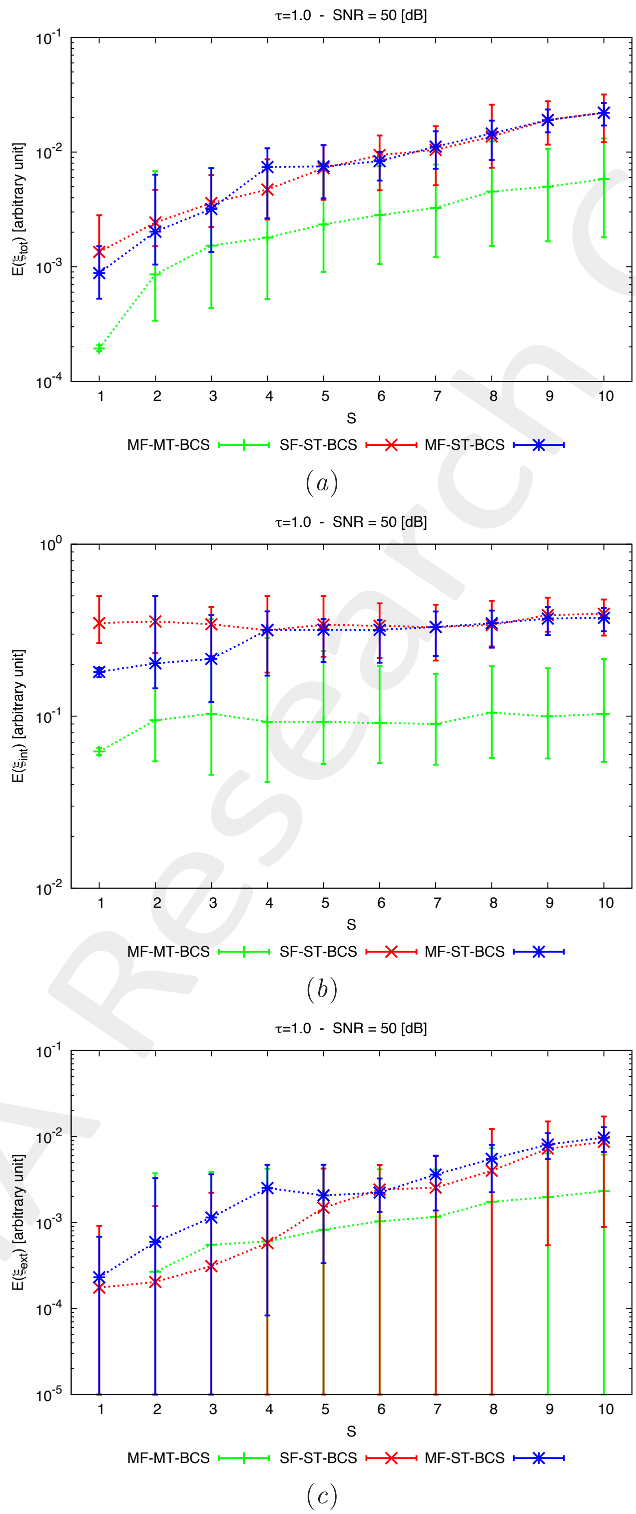

Figure 87. *Statistical analysis* $[K = 14, \varepsilon_r = 2.0]$ - Behaviour of mean, maximum and minimum of the error figures as a function of S (sparsity factor) of the total error ξ_{tot} (a), internal error ξ_{int} (b) and external error ξ_{ext} (c).

Statistical Analysis - Error Figures - BCS Comparison - $SNR = 20$ [dB]

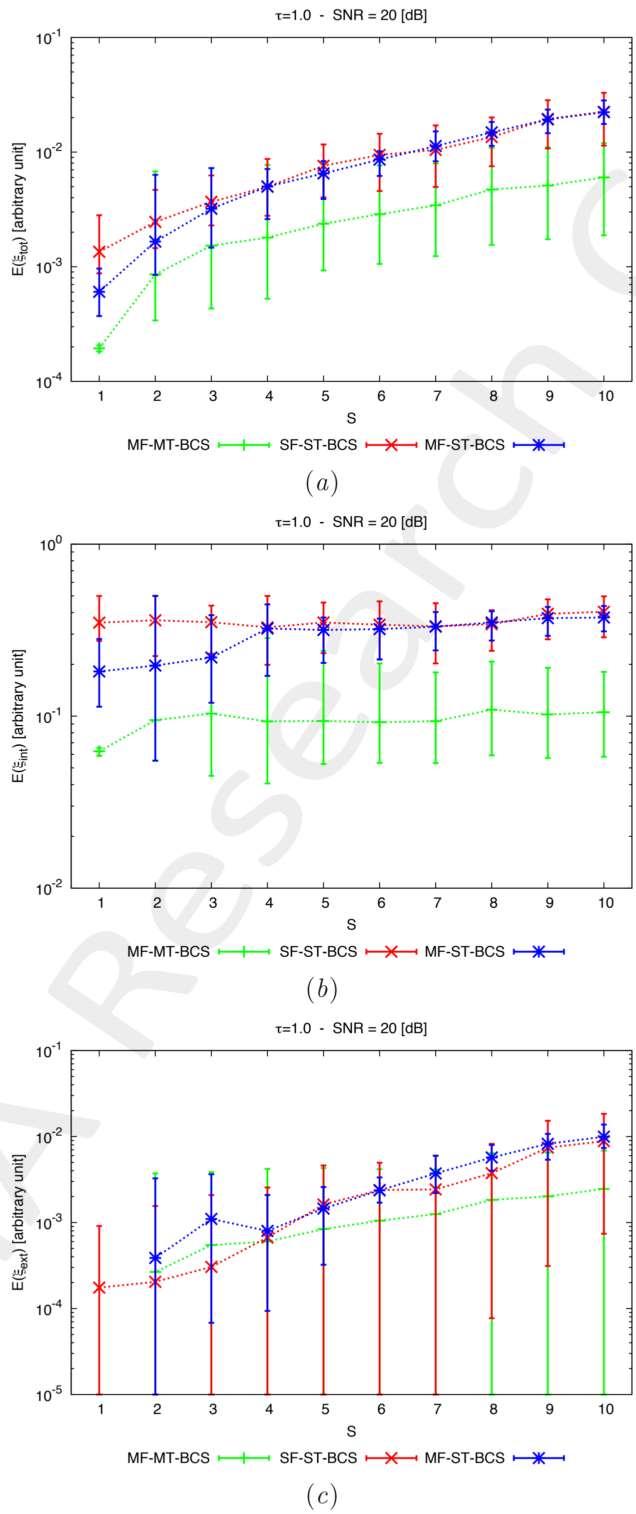

Figure 88. *Statistical analysis* $[K = 14, \varepsilon_r = 2.0]$ - Behaviour of mean, maximum and minimum of the error figures as a function of S (sparsity factor) of the total error ξ_{tot} (a), internal error ξ_{int} (b) and external error ξ_{ext} (c).

Statistical Analysis - Error Figures - BCS Comparison - $SNR = 10$ [dB]

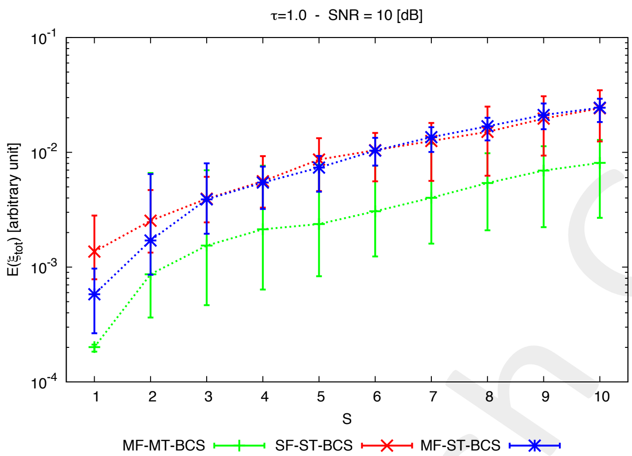

(a)

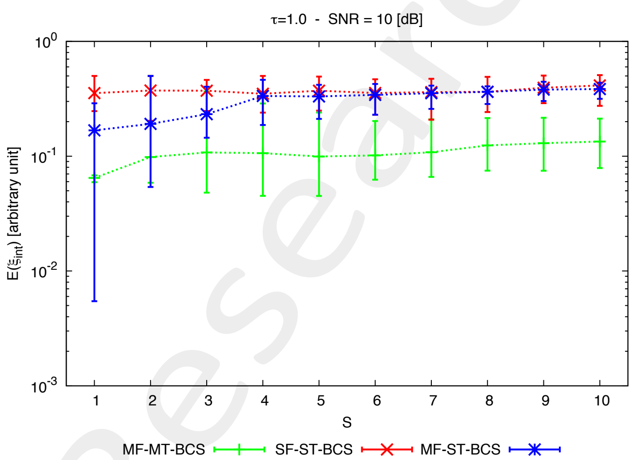

(b)

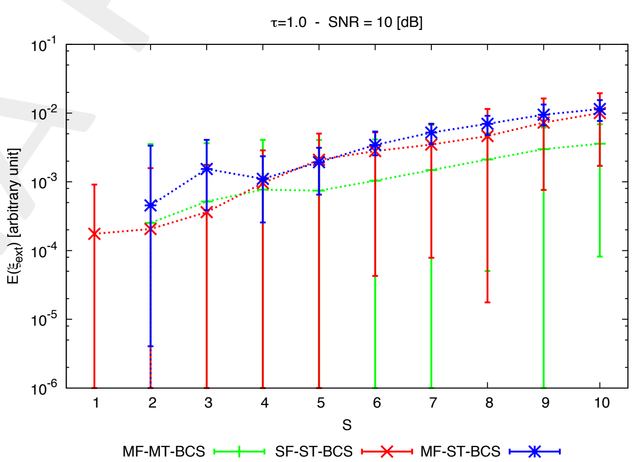

(c)

Figure 89. *Statistical analysis* $[K = 14, \varepsilon_r = 2.0]$ - Behaviour of mean, maximum and minimum of the error figures as a function of S (sparsity factor) of the total error ξ_{tot} (a), internal error ξ_{int} (b) and external error ξ_{ext} (c).

Statistical Analysis - Error Figures - BCS Comparison - $SNR = 5$ **[dB]**

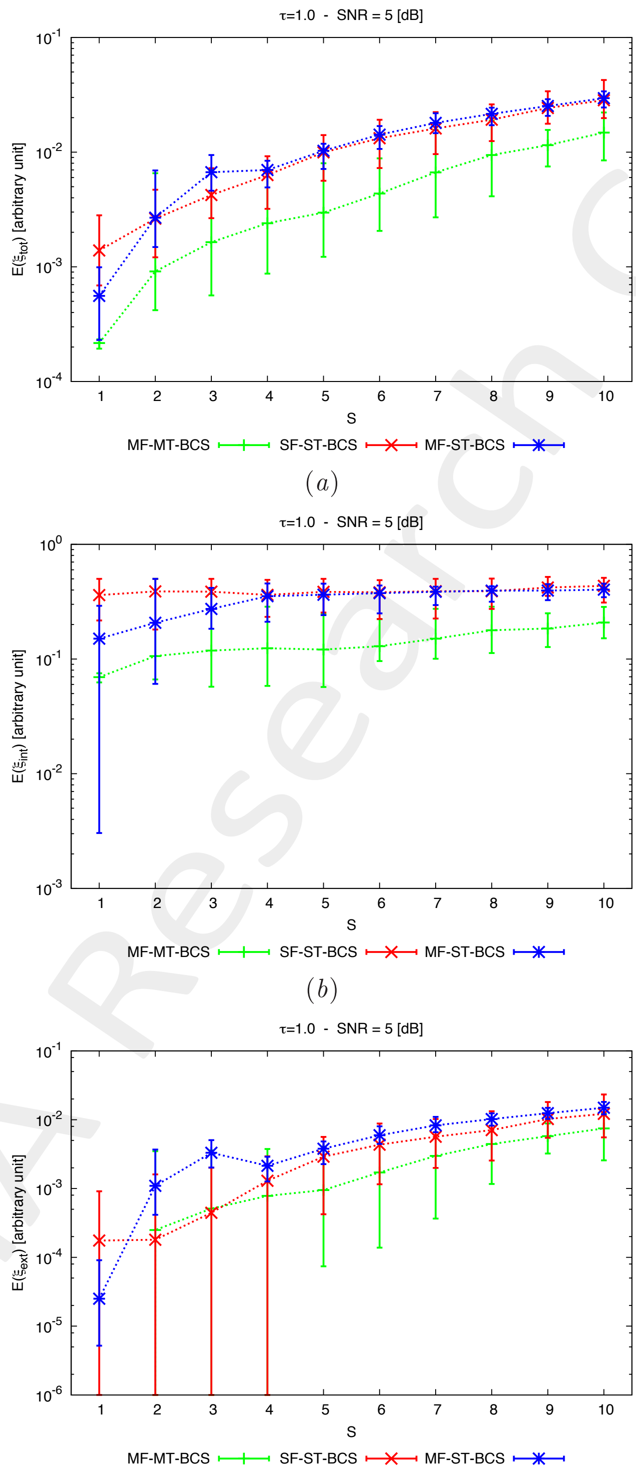

Figure 90. *Statistical analysis* $[K = 14,\ \varepsilon_r = 2.0]$ - Behaviour of mean, maximum and minimum of the error figures as a function of S (sparsity factor) of the total error ξ_{tot} (a), internal error ξ_{int} (b) and external error ξ_{ext} (c).

References

[1] G. Oliveri, P. Rocca, and A. Massa, "A Bayesian compressive sampling-based inversion for imaging sparse scatterers," IEEE Trans. Geosci. Remote Sens., vol. 49, no. 10, pp. 3993-4006, Oct. 2011.

[2] L. Poli, G. Oliveri, P.-P. Ding, T. Moriyama, and A. Massa, "Multifrequency Bayesian compressive sensing methods for microwave imaging," Journal of the Optical Society of the America A, vol. 31, no. 11, pp. 2415-2428, 2014.

[3] G. Oliveri, N. Anselmi, and A. Massa, "Compressive sensing imaging of non-sparse 2D scatterers by a total-variation approach within the Born approximation," IEEE Trans. Antennas Propag., vol. 62, no. 10, pp. 5157-5170, Oct. 2014.

[4] L. Poli, G. Oliveri, and A. Massa, "Imaging sparse metallic cylinders through a Local Shape Function Bayesian Compressive Sensing approach," Journal of Optical Society of America A, vol. 30, no. 6, pp. 1261-1272, 2013.

[5] F. Viani, L. Poli, G. Oliveri, F. Robol, and A. Massa, "Sparse scatterers imaging through approximated multitask compressive sensing strategies," Microwave Opt. Technol. Lett., vol. 55, no. 7, pp. 1553-1558, Jul. 2013.

[6] L. Poli, G. Oliveri, P. Rocca, and A. Massa, "Bayesian compressive sensing approaches for the reconstruction of two-dimensional sparse scatterers under TE illumination," IEEE Trans. Geosci. Remote Sensing, vol. 51, no. 5, pp. 2920-2936, May 2013.

[7] L. Poli, G. Oliveri, and A. Massa, "Microwave imaging within the first-order Born approximation by means of the contrast-field Bayesian compressive sensing," IEEE Trans. Antennas Propag., vol. 60, no. 6, pp. 2865-2879, Jun. 2012.

[8] G. Oliveri, L. Poli, P. Rocca, and A. Massa, "Bayesian compressive optical imaging within the Rytov approximation," Optics Letters, vol. 37, no. 10, pp. 1760-1762, 2012.

[9] L. Poli, G. Oliveri, F. Viani, and A. Massa, "MT-BCS-based microwave imaging approach through minimum-norm current expansion," IEEE Trans. Antennas Propag., vol. 61, no. 9, pp. 4722-4732, Sep. 2013.

[10] G. Oliveri, P.-P. Ding, and L. Poli "3D crack detection in anisotropic layered media through a sparseness-regularized solver," IEEE Antennas Wireless Propag. Lett., in press.

[11] M. Salucci, G. Oliveri, A. Randazzo, M. Pastorino, and A. Massa, "Electromagnetic subsurface prospecting by a multifocusing inexact Newton method within the second-order Born approximation," J. Opt. Soc. Am. A., vol. 31, no. 6, pp. 1167-1179, Jun. 2014.

[12] G. Oliveri, L. Lizzi, M. Pastorino, and A. Massa, "A nested multi-scaling inexact-Newton iterative approach for microwave imaging," IEEE Trans. Antennas Propag., vol. 60, no. 2, pp. 971-983, Feb. 2012.

[13] G. Oliveri, A. Randazzo, M. Pastorino, and A. Massa, "Electromagnetic imaging within the contrast-source formulation by means of the multiscaling inexact Newton method," Journal of Optical Society of America A, vol. 29, no. 6, pp. 945-958, 2012.

[14] M. Benedetti, D. Lesselier, M. Lambert, and A. Massa, "Multiple shapes reconstruction by means of multi-region level sets," IEEE Trans. Geosci. Remote Sensing, vol. 48, no. 5, pp. 2330-2342, May 2010.

[15] M. Benedetti, D. Lesselier, M. Lambert, and A. Massa, "A multi-resolution technique based on shape optimization for the reconstruction of homogeneous dielectric objects," Inverse Problems, vol. 25, no. 1, pp. 1-26, Jan. 2009.

[16] T. Moriyama, G. Oliveri, M. Salucci, and T. Takenaka, "A multi-scaling forward-backward time-stepping method for microwave imaging," IEICE Electronics Express, vol. 11, no. 16, pp. 1-12, Aug. 2014.

[17] G. Oliveri and A. Massa, "Bayesian compressive sampling for pattern synthesis with maximally sparse non-uniform linear arrays," IEEE Trans. Antennas Propag., vol. 59, no. 2, pp. 467-481, Feb. 2011.

[18] G. Oliveri, M. Carlin, and A. Massa, "Complex-weight sparse linear array synthesis by Bayesian Compressive Sampling," IEEE Trans. Antennas Propag., vol. 60, no. 5, pp. 2309-2326, May 2012.

[19] G. Oliveri, P. Rocca, and A. Massa, "Reliable Diagnosis of Large Linear Arrays - A Bayesian Compressive Sensing Approach," IEEE Trans. Antennas Propag., vol. 60, no. 10, pp. 4627-4636, Oct. 2012.

[20] F. Viani, G. Oliveri, and A. Massa, "Compressive sensing pattern matching techniques for synthesizing planar sparse arrays," IEEE Trans. Antennas Propag., vol. 61, no. 9, pp. 4577-4587, Sept. 2013.

[21] G. Oliveri, E. T. Bekele, F. Robol, and A. Massa, "Sparsening conformal arrays through a versatile BCS-based method," IEEE Trans. Antennas Propag., vol. 62, no. 4, pp. 1681-1689, Apr. 2014.

[22] M. Carlin, G. Oliveri, and A. Massa, "Hybrid BCS-deterministic approach for sparse concentric ring isophoric arrays," IEEE Trans. Antennas Propag., vol. 63, no. 1, pp. 378-383, Jan. 2015.